

Steady-state spin synchronization through the collective motion of trapped ions

Athreya Shankar,^{1,*} John Cooper,¹ Justin G. Bohnet,² John J. Bollinger,² and Murray Holland¹

¹*JILA, NIST, and Department of Physics, University of Colorado Boulder, Boulder, Colorado 80309-0440 USA*

²*Time and Frequency Division, National Institute of Standards and Technology, Boulder, Colorado 80305, USA*

(Dated: September 18, 2018)

Ultranarrow-linewidth atoms coupled to a lossy optical cavity mode synchronize, i.e. develop correlations, and exhibit steady-state superradiance when continuously repumped. This type of system displays rich collective physics and promises metrological applications. These features inspire us to investigate if analogous spin synchronization is possible in a different platform that is one of the most robust and controllable experimental testbeds currently available: ion-trap systems. We design a system with a primary and secondary species of ions that share a common set of normal modes of vibration. In analogy to the lossy optical mode, we propose to use a lossy normal mode, obtained by sympathetic cooling with the secondary species of ions, to mediate spin synchronization in the primary species of ions. Our numerical study shows that spin-spin correlations develop, leading to a macroscopic collective spin in steady-state. We propose an experimental method based on Ramsey interferometry to detect signatures of this collective spin; we predict that correlations prolong the visibility of Ramsey fringes, and that population statistics at the end of the Ramsey sequence can be used to directly infer spin-spin correlations.

PACS numbers: 37.10.Ty, 42.50.Nn, 03.65.Yz, 05.45.Xt

I. INTRODUCTION

Steady-state synchronization of atomic dipoles forms the foundation for ultra-stable optical lasers utilizing narrow-linewidth atoms coupled to a lossy cavity mode. Such lasers have recently been proposed [1, 2] and experimentally explored with a Raman system [3], and in a true narrow-linewidth transition in strontium [4]. The cavity mode acts as a channel for synchronization of the atomic dipoles (spins) resulting in a macroscopic collective dipole in steady-state composed of correlated atoms [2]. Synchronization here refers to the development of a preferred relative phase (correlations) between every pair of spins. The output light is a result of collective spontaneous emission of this macroscopic dipole, as in the case of Dicke superradiance [5], with the difference that the superradiance is in steady-state with repumping of the atoms balancing the cavity loss.

Steady-state superradiant lasers provide a platform for studying quantum synchronization and have applications as ultra-stable optical frequency sources. The linewidth of the output light is determined by the decay rate of the narrow-linewidth transition [1], exploiting the all-to-all pair-wise phase-locking of a large number of spins to drastically reduce the linewidth. The exciting features of cavity steady-state superradiance, such as the narrow linewidth light and the spin synchronization, motivate us to ask whether a superradiance model can be used to synchronize quantum ensembles in other platforms, and if such systems could exhibit interesting physics and have possible applications.

Ion-trap systems have become a robust platform for experiments related to quantum computing, simulation

and metrology [6–8], making them an excellent candidate for studies of spin synchronization. Ion traps have long trapping times, routinely trapping ions for several hours. The incoherent repumping, crucial to maintain steady-state superradiance, introduces recoil heating which can kick neutral atoms out of the shallow traps used in optical cavities. Complicated schemes must be used to mimic a steady-state number of atoms in this situation. However, this problem is negligible in ion traps which have much deeper trapping potentials. Further, ions in a trap are distinguishable because of the large spacings ($\sim \mu\text{m}$) between them, enabling access to individual spins for direct measurement of spin-spin correlations.

One approach to synchronizing ions is to place ion traps in optical cavities, allowing the ions to interact with the cavity mode. However, the low density of trapped ions makes it difficult to couple more than $O(10^3)$ ions to the cavity, prohibiting the large collective cooperativities possible with neutral atoms, where 10^5 to 10^6 atoms are routinely used.

A second approach is to couple ions through the normal modes of vibration of the trap, arising out of the Coulomb interactions between the ions. Like optical cavity modes, these normal modes are a natural coupling channel for interactions between distant particles. A normal mode of vibration and an optical cavity mode are both bosonic modes that can be described in the language of quantum harmonic oscillators [9]. Laser beams can be used to couple the electronic and motional degrees of freedom in different ways [10, 11]. Ion traps also enable us to engineer a dedicated dissipative channel with tunable properties: a subset of ions can be used to sympathetically cool the entire crystal [12–14], removing phonons from the normal modes analogous to lossy mirrors removing photons from the cavity mode. The phonon loss rate and equilibrium phonon number (temperature) can be controlled by

* athreya.shankar@colorado.edu

adjusting the power and detuning of the cooling laser.

In this paper, we follow this second approach, to design and analyze a scheme for generating spin synchronization in an ion trap, by coupling a collection of continuously repumped ions with a heavily damped normal mode of vibration. This scheme offers several features that are quite novel in ion trap systems. Most protocols in ion traps use Hamiltonian interactions. However, the present approach promises to synchronize a mesoscopic (20 to 500) number of ions using dissipation as a crucial ingredient. Our proposal is enabled by recent demonstrations of control over hundreds of ions in Penning traps [15], as well as improvements in radio frequency (RF) traps [16, 17] that make it possible to control tens of ions in these traps. The key ingredients have also been implemented with a small number of ions in RF traps for preparing entangled states, demonstrating the feasibility of our scheme [18].

Spin synchronization from steady-state superradiance can enhance metrology with trapped ions. Theoretical studies have shown that when continuously repumped spins interact with a heavily damped cavity mode during the interrogation time of a Ramsey pulse sequence, the resulting Ramsey fringes can decay at a rate much slower than the decay and dephasing rates for unsynchronized atoms [19]. Implementing such a protocol using a damped normal mode in an ion trap could mitigate inhomogeneous broadening effects, and improve the capability of trapped ions for sensing, for example, of time-varying magnetic fields.

This paper is organized as follows. In Sec. II, we consider a model of two species of ions loaded in an ion trap that can be used to explore spin synchronization mediated by a damped normal mode. In Sec. III, we consider a specific example of an ion trap system where this scheme could be implemented. We numerically investigate this model system, comparing the results with the corresponding atom-cavity model. We look for signatures of synchronization brought about by steady-state superradiance such as the pair-wise correlations between ions. We also propose an experimental scheme to observe features of the collective dipole based on a Ramsey pulse sequence. We show that the collective dipole results in Ramsey fringes that decay with a slower rate than that expected from incoherent repumping, and the variance in the population readout at the end of the Ramsey sequence directly measures the steady-state spin-spin correlations. We then briefly touch on how this model can be a potential candidate for improving metrology with ion trap systems. We conclude by summarizing our results in Sec. IV, and indicating possible future directions.

II. MODEL

There are three crucial ingredients to generate steady-state superradiance in a cavity (see Fig. 1): (a) a heavily damped cavity mode, (b) a Jaynes-Cummings interaction between two-level atoms and the nearly-resonant

cavity mode, and (c) incoherent repumping of the two-level atoms to maintain steady-state.

In Fig. 1, we schematically show the mapping of the problem of cavity steady-state superradiance onto an ion trap system. We consider two species of ions, τ (secondary) and σ (primary), loaded in an ion trap [20]. The two species could be, for example, two different elements, or isotopes of the same element. The system has a total of $N = N_\tau + N_\sigma$ ions, and therefore the transverse (z -axis) motion of any ion can be described using the N transverse normal modes of the system. The τ ions are used to sympathetically cool the normal modes of vibration of the system of ions. The σ ions provide the effective spins that synchronize through the interaction with a damped normal mode.

In Sec. II A, we demonstrate that Doppler cooling of the two-level τ ions leads to an effective damping of the normal modes. The effective dynamics for each mode can be described as an interaction of a single-mode harmonic oscillator with a reservoir at a finite temperature. Then, in Sec. II B, we derive the interaction of the three-level σ ions with a pair of off-resonant Raman beams, taking into account the effects of dissipative processes. When the difference frequency of the Raman beams is suitably tuned, this interaction models a Jaynes-Cummings type interaction between an effective spin-1/2 system and a particular normal mode. Finally, in Sec. II C, we consider the interaction between the spin-1/2 systems formed by the σ ions and the strongly damped normal modes. We obtain an effective dynamics for these spin-1/2 systems, that consists only of spin-spin interactions. We then compare our ion trap model with the model for cavity steady-state superradiance [21], and highlight the similarities in the dynamics, as well as the differences.

A. Doppler cooling of τ ions

The τ ions are two-level systems that are placed at the node of a standing-wave cooling laser [22]. A traveling-wave laser may be used for cooling provided the achieved steady-state temperature, characterized by the mean occupation number of the normal modes, is not very high. The level diagram of a τ ion is shown in Fig. 2. The $|e\rangle \leftrightarrow |g\rangle$ transition is dipole allowed, and can be used to Doppler cool the normal modes of the system. The level $|e\rangle$ decays to $|g\rangle$ at a rate Γ_τ . The cooling laser has a Rabi frequency of Ω_τ and a wavevector $\vec{k}_{\text{sw}} = k_{\text{sw}}\hat{z}$. We use the notation τ^\pm, τ^z to denote the Pauli spin matrices associated with the τ ions.

The master equation for the interaction of the N_τ τ ions and N normal modes with the cooling laser is

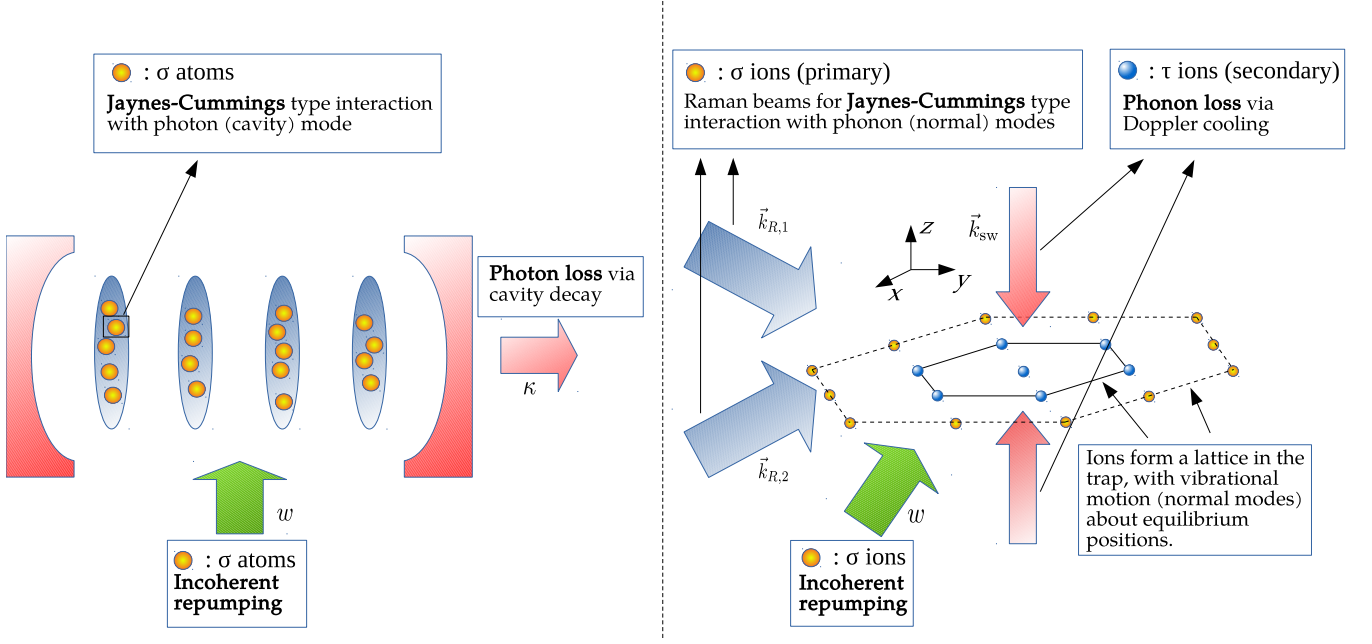


FIG. 1. (color online) Mapping cavity steady-state superradiance onto an ion trap system. In the left panel, we show the model for cavity steady-state superradiance, where the cavity mode serves as a mediator for collective decay of the spins formed by the σ atoms. In the right panel, we show the ion trap system where a normal mode of vibration serves as a mediator for collective decay of the spins formed by the σ ions. The figure illustrates the model with a 2-dimensional crystal. More generally our model can also be applied to 1D crystals of ions.

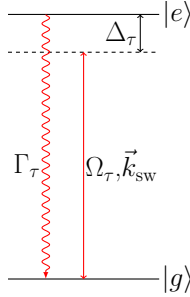


FIG. 2. (color online) Level diagram of a τ ion. The τ ions are driven using a cooling laser that is red detuned from the dipole allowed $|e\rangle \leftrightarrow |g\rangle$ transition. This results in cooling of the normal modes of vibration of the ion trap system.

$$\begin{aligned} \dot{\rho}_{\tau,\text{ph}} = & -i[H_{\tau,\text{ph}}, \rho_{\tau,\text{ph}}] \\ & + \frac{\Gamma_{\tau}}{2} \sum_m \int_{-1}^1 du W(u) \mathcal{D}[\tau_m^- e^{-ik_{\tau} z_m u}] \rho_{\tau,\text{ph}}. \end{aligned} \quad (1)$$

Here, $\rho_{\tau,\text{ph}}$ is the density matrix describing the τ -spins and the normal modes (the subscript “ph” is shorthand for “phonons”). Throughout this paper, we have set $\hbar = 1$, unless we explicitly specify otherwise. The notation $\mathcal{D}[O]$ is used to represent the standard Lindblad

dissipator, i.e., $\mathcal{D}[O]\rho = 2O\rho O^{\dagger} - O^{\dagger}O\rho - \rho O^{\dagger}O$. The second term on the RHS of Eq. (1) accounts for the dissipation due to spontaneous emission, and its effects on the transverse motion of the ions. The wavevector \vec{k}_{τ} of the spontaneously emitted photon makes an angle $\theta = \cos^{-1}u$ with the z -axis, where the distribution of the angles is given by the normalized, even function $W(u)$. The transverse position of the ion m is denoted by z_m .

In a frame rotating at the cooling laser frequency, the Hamiltonian $H_{\tau,\text{ph}}$ in Eq. (1) is

$$\begin{aligned} H_{\tau,\text{ph}} = & -\frac{1}{2}\Delta_{\tau} \sum_m \tau_m^z + \sum_n \omega_n b_n^{\dagger} b_n \\ & + \frac{\Omega_{\tau}}{2} \sum_m \sin(k_{\text{sw}} z_m) (\tau_m^- + \tau_m^+), \end{aligned} \quad (2)$$

where $\Delta_{\tau} = \omega_{\text{sw}} - (\omega_e - \omega_g)$ is the detuning of the cooling laser. The frequency of the normal mode n is given by ω_n , and its annihilation and creation operators are b_n and b_n^{\dagger} .

For small detunings, $k_{\text{sw}} \approx k_{\tau} \equiv k$. The dimensionless quantity kz_m for the ion m can be expressed in terms of the normal modes of the system as

$$kz_m = \sum_n \eta_n^{\tau} \mathcal{M}_{mn} (b_n + b_n^{\dagger}), \quad (3)$$

and captures the spread in the position of the ion relative to the wavelength of the light it interacts with. The quantity $\eta_n^\tau = k\sqrt{\frac{\hbar}{2m_\tau\omega_n}}$ is the Lamb-Dicke parameter [23] for the normal mode n . The equilibrium positions of the σ and τ ions are due to a balance between the trap potential and the Coulomb interactions between the ions. Displacement of an ion from equilibrium results in simple harmonic motion. The matrix \mathcal{M} diagonalizes the potential energy matrix (written in mass-weighted coordinates) of this simple harmonic motion. The frequencies ω_n of the normal modes are obtained from the eigenvalues of this potential energy matrix [24].

In the Lamb-Dicke regime ($((kz_m)^2)^{1/2} \ll 1$) [23], we can expand the RHS of the master equation in powers of $\{\eta_n^\tau\}$. When the decay rate Γ_τ is large compared with the couplings $\{\Omega_\tau\eta_n^\tau\}$ between the system of normal modes and the reservoir of τ ions, second-order perturbation theory and a Markov approximation can be used to arrive at an effective master equation for the damping of the system of normal modes (see Appendix A). The cooling introduces couplings between the normal modes, resulting in a new dressed set of normal modes that are decoupled from each other. For simplicity, here we neglect couplings between different modes, and approximate the bare modes to be decoupled from each other¹. Then, the effective master equation that describes the damping of normal modes is given by

$$\dot{\mu}_{\text{ph}} = -i \left[\sum_n \omega'_n b_n^\dagger b_n, \mu_{\text{ph}} \right] + \sum_n D_n^- \mathcal{D}[b_n] \mu_{\text{ph}} + \sum_n D_n^+ \mathcal{D}[b_n^\dagger] \mu_{\text{ph}}, \quad (4)$$

where

$$\begin{aligned} \omega'_n &= \omega_n + R_n^-(\Delta_\tau + \omega_n) + R_n^+(\Delta_\tau - \omega_n), \text{ and} \\ D_n^\pm &= R_n^\pm \frac{\Gamma_\tau}{2} \text{ with} \\ R_n^\pm &= \frac{\sum_m (\frac{1}{2}\Omega_\tau\eta_m^\tau \mathcal{M}_{mn})^2}{\frac{\Gamma_\tau^2}{4} + (\Delta_\tau \mp \omega_n)^2}. \end{aligned} \quad (5)$$

Here μ_{ph} is the density matrix describing the normal modes. To draw an analogy with cavity QED models, it is useful to define a cooling rate per mode $\kappa_n = 2(D_n^- - D_n^+)$ and a mean occupation number per mode $\bar{n}_n = D_n^+ / (D_n^- - D_n^+)$. Then Eq. (4) can be written as

$$\begin{aligned} \dot{\mu}_{\text{ph}} &= -i \left[\sum_n \omega'_n b_n^\dagger b_n, \mu_{\text{ph}} \right] \\ &+ \sum_n \frac{\kappa_n(\bar{n}_n + 1)}{2} \mathcal{D}[b_n] \mu_{\text{ph}} + \sum_n \frac{\kappa_n \bar{n}_n}{2} \mathcal{D}[b_n^\dagger] \mu_{\text{ph}}. \end{aligned} \quad (6)$$

Eq. (6) describes the decay of N individual harmonic oscillators with frequencies $\{\omega_n\}$, each respectively in contact with a reservoir in a thermal state with mean occupation number \bar{n}_n , at rates κ_n [25].

B. Interaction of σ ions with Raman beams

The level diagram of a σ ion is shown in Fig. 3. The $|1\rangle \leftrightarrow |2\rangle$ and $|3\rangle \leftrightarrow |2\rangle$ transitions are dipole allowed, but the $|1\rangle \leftrightarrow |3\rangle$ transition is dipole forbidden. A pair of Raman beams are used to drive the $|1\rangle \leftrightarrow |2\rangle$ and $|3\rangle \leftrightarrow |2\rangle$ transitions. Their wavevectors, frequencies and Rabi coupling strengths are respectively $\vec{k}_{R,1}, \omega_{R,1}, g_1$ and $\vec{k}_{R,2}, \omega_{R,2}, g_2$. The Rabi coupling strengths have a position dependency arising from the traveling-wave Raman beams, i.e.

$$g_1 = g_{1,0} e^{i\vec{k}_{R,1} \cdot \vec{x}}, \text{ and } g_2 = g_{2,0} e^{i\vec{k}_{R,2} \cdot \vec{x}}. \quad (7)$$

The difference wavevector $\vec{k}_\sigma = \vec{k}_{R,1} - \vec{k}_{R,2}$ is along the (transverse) z -axis. The level $|2\rangle$ decays to levels $|1\rangle$ and $|3\rangle$ at rates Γ_1 and Γ_2 respectively. The Raman beams operate in a regime where they are far detuned from the transitions they drive: $\Delta_1 = \omega_{R,1} - (\omega_2 - \omega_1), \Delta_2 = \omega_{R,2} - (\omega_2 - \omega_3) \gg |g_1|, |g_2|, \Gamma_1, \Gamma_2$.

The master equation for a σ -ion interacting with Raman beams is given by

$$\dot{\rho}_\sigma = -i[H_\sigma, \rho_\sigma] + \frac{\Gamma_1}{2} \mathcal{D}[\sigma_{12}] \rho_\sigma + \frac{\Gamma_2}{2} \mathcal{D}[\sigma_{32}] \rho_\sigma, \quad (8)$$

where ρ_σ is the density matrix for a single σ -ion.

The Hamiltonian appearing in Eq. (8) is

$$H_\sigma = \Delta_1 \sigma_{11} + \Delta_2 \sigma_{33} + \left(\frac{g_1}{2} \sigma_{21} + \frac{g_2}{2} \sigma_{23} + \text{h.c.} \right), \quad (9)$$

where we use the notation $\sigma_{ij} = |i\rangle \langle j|, i, j = 1, 2, 3$ to represent operators acting on the electronic levels of the σ ion.

Driving this three-level system in a far detuned regime results in Rabi oscillations between levels $|1\rangle$ and $|3\rangle$. While this is a well known result [23], it is important for our study to consider the dissipative processes that arise because of the scattering from $|2\rangle$. We use a recently developed Schrieffer-Wolff formalism for dissipative systems [26], which is a projection operator method,

¹ See Eq. (A11) and the subsequent remarks in Appendix A.

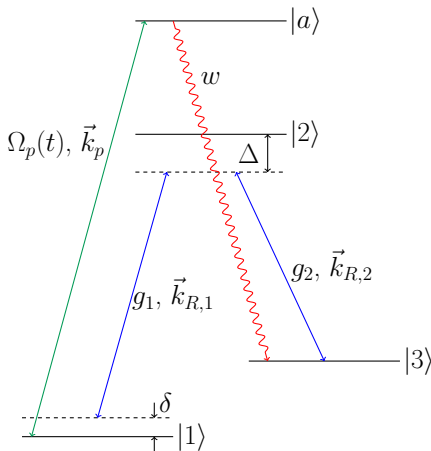


FIG. 3. (color online) Level diagram of a σ ion. The three level configuration $\{|1\rangle, |2\rangle, |3\rangle\}$ is used to drive stimulated Raman transitions in a far detuned regime, giving rise to an effective two-level system in the $\{|1\rangle, |3\rangle\}$ manifold. The detuning δ can be adjusted to drive red sideband transitions coupling the electronic dynamics with an external normal mode of vibration. Incoherent pumping through an excited state $|a\rangle$ replenishes energy lost via Doppler cooling (not shown here) of the normal mode.

to rigorously obtain the effective dynamics of the two-level system formed by the $\{|1\rangle, |3\rangle\}$ manifold.

The use of this formalism in the present case is detailed in Appendix B. We then get a description of the effective dynamics in the $\{|1\rangle, |3\rangle\}$ manifold. We denote operators in this space using Pauli spin matrices: $\sigma^z = \sigma_{33} - \sigma_{11}$, $\sigma^+ = \sigma_{31}$, $\sigma^- = \sigma_{13}$. For a collection of σ ions, the master equation describing the dynamics in the $\{|1\rangle, |3\rangle\}$ manifold of these ions is then

$$\begin{aligned} \dot{\mu} = & -i[H^{\text{eff}}, \mu] + \frac{\Gamma_{31}}{2} \sum_l \mathcal{D}[\sigma_l^-] \mu \\ & + \frac{\Gamma_{13}}{2} \sum_l \mathcal{D}[\sigma_l^+] \mu + \frac{\Gamma_d}{8} \sum_l \mathcal{D}[\sigma_l^z] \mu, \end{aligned} \quad (10)$$

where

$$H^{\text{eff}} = -\frac{1}{2} \delta_R \sum_l \sigma_l^z + \sum_l \left(\frac{\Omega_{R,l}(z_l)}{2} \sigma_l^+ + \text{h.c.} \right). \quad (11)$$

Here, μ is the density matrix for the effective spin-1/2 systems formed by the $|1\rangle, |3\rangle$ manifolds of the σ ions. In writing Eq. (10), we have omitted certain ‘cross-terms’ [27] which eventually contribute at order $\Gamma_{1,2}^2/\Delta^2 (\ll 1)$ lesser than the interactions of interest. To avoid digressing, we outline the reasoning behind this omission in Appendix B. We have introduced several new symbols in Eq. (10), which are explained in Table I.

At this point, we consider a collection of N_σ σ ions and N_τ τ ions loaded in an ion trap. The collection of ions has $N = N_\sigma + N_\tau$ normal modes in total. The

TABLE I. Symbols used in writing the effective master equation for the σ ions (Eq. (10))

Symbol	Description	Expression
δ_R	effective detuning	$(\Delta_1 + \frac{ g_1 ^2}{4\Delta_1}) - (\Delta_2 + \frac{ g_2 ^2}{4\Delta_2})$
Ω_R	effective Rabi frequency	$\frac{g_1 g_2^*}{4} \left(\frac{1}{\Delta_1} + \frac{1}{\Delta_2} \right)$
Δ	average detuning	$\frac{\Delta_1 + \Delta_2}{2}$
Γ_{31}	effective spontaneous emission	$\Gamma_1 \frac{ g_2 ^2}{4\Delta_2^2}$
Γ_{13}	effective incoherent repumping	$\Gamma_2 \frac{ g_1 ^2}{4\Delta_1^2}$
Γ_d	effective dephasing	$\Gamma_1 \frac{ g_1 ^2}{4\Delta_1^2} + \Gamma_2 \frac{ g_2 ^2}{4\Delta_2^2}$

σ ions with index $l, l \in \{1, \dots, N_\sigma\}$ have an effective Rabi frequency $\Omega_{R,l}(z_l) = \Omega_R^0 e^{ik_\sigma z_l}$. Once again, the dimensionless quantity $k_\sigma z_l$ for ion l can be expressed in terms of the normal modes of the system as

$$k_\sigma z_l = \sum_n \eta_n^\sigma \mathcal{M}_{ln} (b_n + b_n^\dagger), \quad (12)$$

where the quantity $\eta_n^\sigma = k_\sigma \sqrt{\frac{\hbar}{2m_\sigma \omega_n}}$ is the Lamb-Dicke parameter for the normal mode n .

In the Lamb-Dicke regime ($(\langle (k_\sigma z_l)^2 \rangle)^{1/2} \ll 1$), the effective Rabi frequency $\Omega_{R,l}$ can be expanded up to first order as

$$\Omega_{R,l}(z_l) \approx \Omega_R^0 + i\Omega_R^0 \sum_n \eta_n^\sigma \mathcal{M}_{ln} (b_n + b_n^\dagger). \quad (13)$$

The Raman lasers are now tuned to the red sideband [23] by adjusting the effective detuning δ_R . If $|\Omega_R^0| \ll |\delta_R| \sim \omega_n$, the contributions from the carrier and blue sideband interactions can be neglected, as the coherences associated with these processes are $O(\Omega_R^0/\delta_R)$ and $O(\Omega_R^0 \eta_n^\sigma/\delta_R)$ respectively. The effective Hamiltonian in Eq. (10) is approximately

$$\begin{aligned} H^{\text{eff}} \approx & -\frac{1}{2} \delta_R \sum_l \sigma_l^z + \sum_n \omega_n b_n^\dagger b_n \\ & + \sum_l \sum_n (\mathcal{F}_{ln} \sigma_l^+ b_n + \text{h.c.}), \end{aligned} \quad (14)$$

where $\mathcal{F}_{ln} = i\Omega_R^0 \eta_n^\sigma \mathcal{M}_{ln}/2$ is the effective coupling strength for a Jaynes-Cummings (JC) type interaction between ion l and normal mode n . We have included the self-energy terms for the normal modes, since the master equation (10) now describes the combined system of σ ions and the normal modes. Note that \mathcal{F}_{ln} is smaller than the effective Rabi frequency Ω_R^0 by a factor $\eta_n^\sigma \mathcal{M}_{ln}$. This is the reason why the (usually) small dissipative processes arising from the stimulated Raman process could be important in our study.

C. Effective spin-spin model for σ ions

In Sec. II B, we obtained the effective dynamics for the interaction of the σ ions with the Raman lasers. The σ ions, henceforth treated as effective spin-1/2 systems, interact with the normal modes through a Jaynes-Cummings type interaction. Earlier, in Sec. II A, the Doppler cooling of the τ ions was used to derive an effective damping for the normal modes. In this section, we proceed by describing the interaction of the σ ions with these damped set of normal modes.

The master equation for the interaction of the σ -ions with the damped set of normal modes is given by

$$\begin{aligned} \dot{\rho}_{\sigma,\text{ph}} &= -i[H_{\sigma,\text{ph}}, \rho_{\sigma,\text{ph}}] \\ &+ \sum_n \frac{\kappa_n(\bar{n}_n + 1)}{2} \mathcal{D}[b_n] \rho_{\sigma,\text{ph}} + \sum_n \frac{\kappa_n \bar{n}_n}{2} \mathcal{D}[b_n^\dagger] \rho_{\sigma,\text{ph}}, \end{aligned} \quad (15)$$

where

$$\begin{aligned} H_{\sigma,\text{ph}} &= -\frac{1}{2} \sum_l \delta_R \sigma_l^z + \sum_n \omega'_n b_n^\dagger b_n \\ &+ \sum_l \sum_n (\mathcal{F}_{ln} \sigma_l^+ b_n + \text{h.c.}). \end{aligned} \quad (16)$$

Here, $\rho_{\sigma,\text{ph}}$ is the density matrix describing the σ -spins and the normal modes.

It is convenient to first transform to an interaction picture with $H_0 = -\delta_R (\frac{1}{2} \sum_l \sigma_l^z + \sum_n b_n^\dagger b_n)$. The Hamiltonian appearing in Eq. (15) in this interaction picture is

$$H_I = \sum_n \tilde{\delta}_n b_n^\dagger b_n + \sum_l \sum_n (\mathcal{F}_{ln} \sigma_l^+ b_n + \text{h.c.}), \quad (17)$$

where $\tilde{\delta}_n = \omega'_n + \delta_R$ is the effective detuning of the normal mode n . We assume that the Raman laser beams are tuned very close to the highest frequency mode, which we take to be the center-of-mass (COM) mode, so that $\delta_R \approx -\omega_{\text{COM}}$. As a result, $|\tilde{\delta}_n|$ is very small for the COM mode and increases with decreasing mode frequency.

The Liouvillian in Eq. (15) can be split into a term \mathcal{L}_R acting on the reservoir of normal modes and a term \mathcal{L}_{SR} that couples the system of σ -spins with this reservoir:

$$\begin{aligned} \dot{\rho}_{\sigma,\text{ph}} &= \mathcal{L}_R \rho_{\sigma,\text{ph}} + \mathcal{L}_{SR} \rho_{\sigma,\text{ph}}, \quad \text{where} \\ \mathcal{L}_R \rho_{\sigma,\text{ph}} &= -i \left[\sum_n \tilde{\delta}_n b_n^\dagger b_n, \rho_{\sigma,\text{ph}} \right] \\ &+ \sum_n \frac{\kappa_n(\bar{n}_n + 1)}{2} \mathcal{D}[b_n] \rho_{\sigma,\text{ph}} + \sum_n \frac{\kappa_n \bar{n}_n}{2} \mathcal{D}[b_n^\dagger] \rho_{\sigma,\text{ph}}, \\ \mathcal{L}_{SR} \rho_{\sigma,\text{ph}} &= -i \left[\sum_l \sum_n (\mathcal{F}_{ln} \sigma_l^+ b_n + \text{h.c.}), \rho_{\sigma,\text{ph}} \right]. \end{aligned} \quad (18)$$

The spin-spin interactions are mediated predominantly by the nearly-resonant COM mode. If the damping rate κ_{COM} of the COM mode is large compared to the collectively-enhanced spontaneous emission rate $N_\sigma \Gamma_{\text{COM}}(1 + \bar{n}_{\text{COM}})$, with $\Gamma_{\text{COM}} = \mathcal{F}_{\text{COM}}^2 / \kappa_{\text{COM}}$, we can obtain an effective master equation for the spin dynamics using second-order perturbation theory and a Markov approximation. The details of this procedure, and an explanation for the validity condition mentioned above are presented in Appendix C. The off-resonant modes are detuned by $\tilde{\delta}_n > \kappa_{\text{COM}}$, ensuring the Markov approximation can be used for the off-resonant modes as well while studying the system on timescales $t \gg \kappa_{\text{COM}}$.

The damping of the normal modes leads to dissipation of energy from the system. To maintain steady-state, energy is replenished by continuous incoherent repumping of the σ -spins at a rate w . This can be achieved by driving the $|1\rangle$ state to an excited state $|a\rangle$, which then rapidly decays to $|3\rangle$. The effective master equation for the density matrix μ_σ of the σ -spins, interacting with a damped set of normal modes and being incoherently repumped is given by

$$\begin{aligned} \dot{\mu}_\sigma &= -i[H_\sigma^{\text{eff}}, \mu_\sigma] \\ &+ \sum_{l,m} \Gamma_{lm}^- (2\sigma_m^- \mu_\sigma \sigma_l^+ - \sigma_l^+ \sigma_m^- \mu_\sigma - \mu_\sigma \sigma_l^+ \sigma_m^-) \\ &+ \sum_{l,m} \Gamma_{lm}^+ (2\sigma_l^+ \mu_\sigma \sigma_m^- - \sigma_m^- \sigma_l^+ \mu_\sigma - \mu_\sigma \sigma_m^- \sigma_l^+) \\ &+ \frac{\Gamma_{31}}{2} \sum_l \mathcal{D}[\sigma_l^-] \mu_\sigma + \left(\frac{w + \Gamma_{13}}{2} \right) \sum_l \mathcal{D}[\sigma_l^+] \mu_\sigma \\ &+ \frac{\Gamma_d}{8} \sum_l \mathcal{D}[\sigma_l^z] \mu_\sigma, \end{aligned} \quad (19)$$

where

$$H_\sigma^{\text{eff}} = \frac{1}{2} \sum_l B_l \sigma_l^z + \sum_{\substack{l,m \\ l \neq m}} J_{lm} \sigma_l^+ \sigma_m^-. \quad (20)$$

The expressions for the coefficients introduced in Eq. (19) are as follows [20]:

$$\begin{aligned} B_l &= - \sum_n \frac{|\mathcal{F}_{ln}|^2}{\frac{\kappa_n^2}{4} + \tilde{\delta}_n^2} \tilde{\delta}_n (1 + 2\bar{n}_n), \\ J_{lm} &= - \sum_n \frac{\mathcal{F}_{ln} \mathcal{F}_{mn}^*}{\frac{\kappa_n^2}{4} + \tilde{\delta}_n^2} \tilde{\delta}_n, \\ \Gamma_{lm}^- &= \sum_n \frac{\mathcal{F}_{ln} \mathcal{F}_{mn}^*}{\frac{\kappa_n^2}{4} + \tilde{\delta}_n^2} \frac{\kappa_n}{2} (1 + \bar{n}_n), \\ \Gamma_{lm}^+ &= \sum_n \frac{\mathcal{F}_{ln} \mathcal{F}_{mn}^*}{\frac{\kappa_n^2}{4} + \tilde{\delta}_n^2} \frac{\kappa_n}{2} \bar{n}_n. \end{aligned} \quad (21)$$

It is useful to gain some physical insight into the terms present in the master equation (19). The terms

$\sum_{l,m} \Gamma_{l,m}^- (2\sigma_m^- \mu_\sigma \sigma_l^+ - \dots)$ and $\sum_{l,m} \Gamma_{l,m}^+ (2\sigma_l^+ \mu_\sigma \sigma_m^- - \dots)$ describe *collective* emission and *collective* absorption of the spins respectively. The emission is stronger than the absorption when the modes are continuously cooled; this is reflected in the expressions for $\Gamma_{l,m}^-, \Gamma_{l,m}^+$ in Eq. (21). The terms of the form $\mathcal{D}[\sigma_l^-] \mu_\sigma$, $\mathcal{D}[\sigma_l^+] \mu_\sigma$ and $\mathcal{D}[\sigma_l^z] \mu_\sigma$ describe spontaneous emission, incoherent repumping and dephasing respectively. The Hamiltonian terms arise because of couplings mediated by the off-resonant normal modes; note that the expressions for B_l and $J_{l,m}$ vanish when the detunings of all the modes are zero. The Hamiltonian terms comprise an effective magnetic field B_l for each spin, as well as pair-wise spin-spin interactions which swap the excitation between the spins.

Eq. (19) reveals that the ion trap model has the key ingredients required to capture steady-state superradiance: collective emission and incoherent repumping. In addition, the ion trap model also replicates the spontaneous emission and dephasing processes that may arise with neutral atoms in a cavity.

There are two important differences between the steady-state superradiance models in an ion-trap and in a cavity. Firstly, the ion trap model also has a collective absorption process, which is present because of the non-zero temperature set by the Doppler cooling. Further, there are Hamiltonian interactions that are mediated by the off-resonant normal modes. This feature is absent in the cavity model where it is usually a good approximation to consider just a single optical mode. In spite of this, the qualitative features of the dynamics in the ion trap model are the same as in the cavity model, as we demonstrate in the next section.

III. A MODEL SYSTEM

A. Trap, ions and laser configurations

We first set the stage by considering a concrete example of an ion trap system. We consider two species of ions, $^{24}\text{Mg}^+$ and $^{25}\text{Mg}^+$, loaded in a Penning trap. The Penning trap allows for controlling large numbers of ions, and also gives a well separated center-of-mass (COM) mode [28] (tens of kilohertz higher than subsequent mode) that makes it possible to mediate superradiant interactions predominantly through a single bosonic mode, as in the cavity case.

Penning traps employ static electric fields and a strong uniform magnetic field $\vec{B} = B\hat{z}$ to confine ions [15]. The static electric fields are generated by applying potentials to electrodes with a common symmetry axis that is aligned with the magnetic field (\hat{z}) axis. The electric fields provide harmonic confinement along the z -axis characterized by a transverse frequency ω_{COM} (this is the frequency of the center-of-mass (COM) mode, which is also the highest frequency mode). The combination

of the electric and magnetic fields leads to $\vec{E} \times \vec{B}$ drift of the ions around the z -axis. This rotation provides the necessary radial confinement. Additional segmented electrodes can be used to apply a rotating potential (‘rotating wall’), and the rotation of the ions can be phase-locked to this ‘rotating wall’ potential, lending stability to the system. For sufficiently weak radial confinement, the ions form a 2D planar crystal with a triangular lattice, as indicated in Fig. 1. For our model parameters, we set the transverse frequency $\omega_{\text{COM}}/2\pi = 2$ MHz, and the lattice spacing between adjacent ions to be $a = 10$ μm . This is possible with a transverse magnetic field of $B \approx 5$ T.

The centrifugal force brought about by the rotation, causing the heavier ions to move outwards, enables separating the two species for different functions of the system. The $^{24}\text{Mg}^+$ ions, to be used for Doppler cooling (τ ions), are located in the center, while the $^{25}\text{Mg}^+$ ions, to be used as effective spin-1/2 systems (σ ions), form hexagonal rings around the inner core of cooling ions. In the high magnetic field regime of the Penning trap, the nuclear spin I essentially decouples from the electronic spin J , and $\{J, m_J\}$ are good quantum numbers to describe the state of the ions. The level structure of these ions, as well as the laser configurations to be used are shown in Fig. 4.

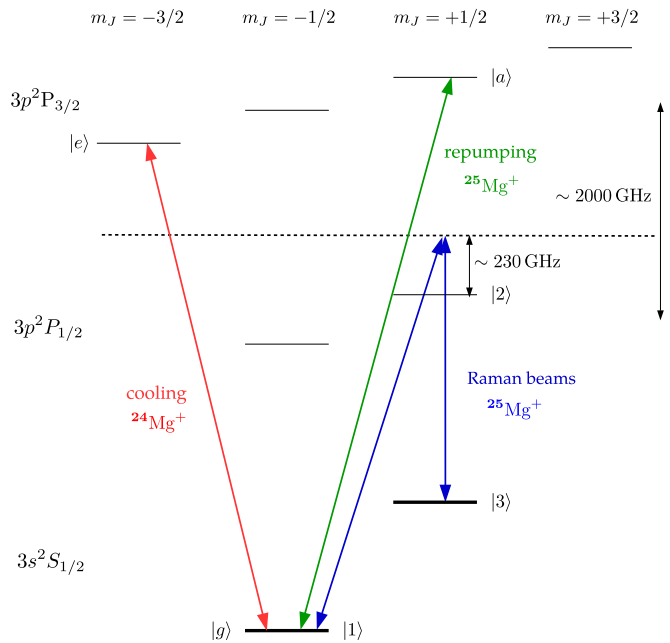


FIG. 4. (color online) Level structure of $^{24}\text{Mg}^+$ and $^{25}\text{Mg}^+$ ions in high field [29, 30]. The hyperfine shifts between the two species are not shown here. The laser configurations to be used are also indicated. The repump laser drives the $3s^2S_{1/2}(m_J = -1/2) \leftrightarrow 3p^2P_{3/2}(m_J = +1/2)$ transition in $^{25}\text{Mg}^+$, and the upper state rapidly decays to $3s^2S_{1/2}(m_J = -1/2)$ and $3s^2S_{1/2}(m_J = +1/2)$ with branching ratios of 1/3 and 2/3 respectively.

1. $^{24}\text{Mg}^+$ (τ ions)

A standing-wave cooling laser (σ^- polarization) is used to drive the $3s^2S_{1/2}(m_J = -1/2) \leftrightarrow 3p^2P_{3/2}(m_J = -3/2)$ transition ($|g\rangle \leftrightarrow |e\rangle$) which has a separation of ~ 280.3 nm. The upper level decays at a rate $\Gamma_\tau/2\pi \approx 41.4$ MHz back to the lower level, thereby providing a cycling transition for Doppler cooling. The cooling laser has a detuning $\Delta_\tau = -\Gamma_\tau/2$ to obtain fast cooling rates. Using a Rabi frequency of $\Omega_\tau/2\pi = 10$ MHz gives a cooling rate of $\kappa_{\text{COM}}/2\pi \sim 5-6$ kHz and a mean occupation $\bar{n}_{\text{COM}} \approx 4.7$ for the COM mode.

2. $^{25}\text{Mg}^+$ (σ ions)

Two Raman beams (Rabi frequencies $|g_1|/2\pi = |g_2|/2\pi \approx 44.7$ MHz), with π and σ^+ polarizations respectively couple the $3s^2S_{1/2}(m_J = +1/2)$ ($|3\rangle$) and the $3s^2S_{1/2}(m_J = -1/2)$ ($|1\rangle$) levels to the $3s^2P_{1/2}(m_J = +1/2)$ ($|2\rangle$) level in a far detuned regime ($\Delta \approx 230$ GHz). Their difference detunings are chosen such that $\delta_R \approx -\omega'_{\text{COM}}$, where ω'_{COM} is the frequency of the COM mode, slightly shifted in the presence of the Doppler cooling. The Raman beams are oriented such that the Lamb-Dicke parameter for the COM mode is $\eta_{\text{COM}}^\sigma \approx 0.1$. A repump laser (σ^+ polarization) drives the $3s^2S_{1/2}(m_J = -1/2) \leftrightarrow 3p^2P_{3/2}(m_J = +1/2)$ transition ($|1\rangle \leftrightarrow |a\rangle$), and the upper level rapidly decays to $|1\rangle$ and $|3\rangle$ with a *relative* branching ratio χ of 0.5. Here, χ is the ratio of the decay rate back to the level $|1\rangle$ and the decay rate to the level $|3\rangle$. To illustrate the important physics, the branching back to the initial state will be ignored initially; however, we will discuss its effects subsequently.

We note here that the Raman beams resonantly tuned to interact with the $^{25}\text{Mg}^+$ ions will not resonantly interact with the $^{24}\text{Mg}^+$ ions; the $^{25}\text{Mg}^+$ ions have a non-zero nuclear spin \vec{I} leading to a hyperfine perturbation Am_Jm_J that changes the level spacing of the effective two-level system by a few gigahertz [29].

B. Results from numerical simulation

In a cavity system, steady-state superradiance can be observed experimentally by measuring the intensity (photons) and phase properties of the output light from the cavity [3]. The corresponding observables in an ion trap are the intensity (phonons) and oscillation phase of the COM mode. While in principle measurable [31, 32], factors like the background phonons from Doppler cooling have to be carefully considered before embarking on such measurements. Standard techniques in ion traps offer convenient ways to directly study the spin degrees of freedom. Steady-state superradiance is characterized by the development of non-zero steady-state spin-spin correlations, leading to the formation of a giant collective spin

which behaves very differently compared to uncorrelated spins. It is this aspect of superradiance that we study numerically and propose techniques for probing via experiments.

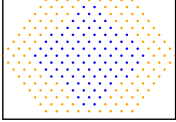
We define an ensemble-averaged (EA) rate $\Gamma_c = (2/N_\sigma^2) \sum_{l,m} (\Gamma_{lm}^- - \Gamma_{lm}^+)$, which plays an analogous role to the net single-atom emission rate into the cavity mode in the superradiant laser [2]. The strength of the Raman beams have been chosen such that the nearly resonant COM mode is strongly damped compared to the collectively-enhanced spontaneous emission rate, i.e. $\kappa_{\text{COM}} \gg N_\sigma \Gamma_c (1 + \bar{n}_{\text{COM}})$. Steady-state superradiance is expected in a regime where the repump strength $w \lesssim N_\sigma \Gamma_c$ [2]. We are interested in the collective behavior of a large number of ions; however, the exact solution is near impossible to compute since the density matrix lives in a 4^{N_σ} dimensional Hilbert space, limiting computation of exact solutions of the master equation to $N_\sigma \lesssim 10$. We use an approximate technique using c -number Langevin equations to analyze this problem. This involves writing the quantum Langevin equations for the spin operators σ_i^\pm, σ_i^z using the master equation (19), obtaining the noise correlations using the Einstein relations [33], and finally making a correspondence between quantum operators and classical c -numbers in order to obtain c -number Langevin equations. This is elaborated in Appendix D. Table II gives the important parameters for numerical simulation of a system comprising $N_\sigma = 124$ and $N_\tau = 93$ ions.

1. Steady-state inversion and spin-spin correlation

The system size (SS) can be specified using the notation (N_σ, N) , where $N = N_\sigma + N_\tau$. An increase in N_σ is accompanied by an increase in N_τ , because for the same laser power, more coolant ions are required to provide fast cooling rates when larger number of ions are present. We will use the notation $\langle \dots \rangle_E$ to denote expectation values that are averaged over the entire ensemble of spins. Figure 5 shows the steady-state EA inversion and spin-spin correlation $(\langle \sigma_i^+ \sigma_j^- \rangle_E)^2$ for three different system sizes: (i) (10, 19), (ii) (48, 91), and (iii) (124, 217). In a minimal cavity model that accounts for only collective emission and incoherent repumping [21], the steady-state values do not change significantly for $N_\sigma \gtrsim 30$ atoms. The inversion and correlation in the cavity case for $N_\sigma = 40$ atoms are shown for comparison. As the system size increases, both the inversion and correlation for the ion trap system become similar to the cavity case [21]: for large N_σ , the inversion grows monotonically with w , and is approximately $1/2$ at $w = 0.5N_\sigma \Gamma_c$ (collective Bloch

² In steady-state, $\langle \sigma_i^\pm \rangle = 0$ for all spins i . Therefore, the correlation $\langle \sigma_i^+ \sigma_j^- \rangle - \langle \sigma_i^+ \rangle \langle \sigma_j^- \rangle$ for every pair i, j of spins is simply $\langle \sigma_i^+ \sigma_j^- \rangle$.

TABLE II. (color online) Summary of important parameters for a numerical simulation, for a system consisting of $N_\sigma = 124$ and $N_\tau = 93$ ions (giving a total of $N = 217$ ions). The table also shows the ion positions used for numerical simulation.

1. Trap	
Input parameters	
a. System size (N_σ, N)	(124, 217)
b. Lattice spacing	10 μm
c. COM mode frequency	2 MHz
d. Ion positions (orange: σ , blue: τ)	
Derived parameters	diagonalize potential energy matrix for above geometry.
2. τ ions	
Input parameters	
a. Upper level decay rate Γ_τ	41.4 ($2\pi \times \text{MHz}$)
b. Transition wavelength	280.3 (nm)
c. Cooling laser detuning Δ_τ	$-\Gamma_\tau/2$
d. Cooling laser Rabi freq. Ω_τ	10 ($2\pi \times \text{MHz}$)
Derived parameters	
a. Cooling rate κ_{COM}	5.1 ($2\pi \times \text{kHz}$)
b. Mean occupation \bar{n}_{COM}	4.7
3. σ ions	
Input parameters	
a. Raman beams $g_1 = g_2$	44.7 ($2\pi \times \text{MHz}$)
b. Average detuning Δ	230 ($2\pi \times \text{GHz}$)
c. Difference detuning δ_R	$-\omega'_{\text{COM}}$
d. Lamb-Dicke parameter η_{COM}	0.1
(sets difference wavevector $ k_\sigma $)	
e. Scattering from $ 2\rangle$: Γ_1, Γ_2	27.27, 13.63 ($2\pi \times \text{MHz}$)
f. Repump w	variable; 0.05 – 1.0 $N_\sigma \Gamma_c$
Derived parameters	
a. Coupling constants $B_l, J_{lm}, \Gamma_{lm}^\pm$	calculate from Eq. (21)
b. Net collective emission rate Γ_c	0.84 ($2\pi \times \text{Hz}$)
c. Spontaneous Raman $\Gamma_{13}, \Gamma_{31}, \Gamma_d$	0.12, 0.24, 0.36 ($2\pi \times \text{Hz}$)

vector is halfway between equator and North Pole). The correlation increases with w , reaches a maximum around $w = 0.5N_\sigma\Gamma_c$, and then decreases with further increase in w . The development of steady-state pair-wise spin-spin correlations implies the phase-locking of spins, and the formation of a giant collective spin, which is a signature of steady-state superradiance. It is reasonable to expect that the ion trap system gives results similar to the zero temperature minimal cavity model as the system size increases; the corrections to the inversion and correlation, due primarily to a non-zero temperature set by \bar{n}_{COM} , scale as $\bar{n}_{\text{COM}}/N_\sigma$. This can be seen by estimating the steady-state values by writing the equations of motion for these expectation values and closing the set of equations by performing a cumulant approximation as was done in Ref. [2, 19].

2. Experimental access: Ramsey fringes

In order to observe this collective spin experimentally, a Ramsey pulse sequence [34] could be used (see Fig. 6(a)). In a traditional Ramsey sequence, the spins initially in the ground state (South Pole of Bloch sphere),

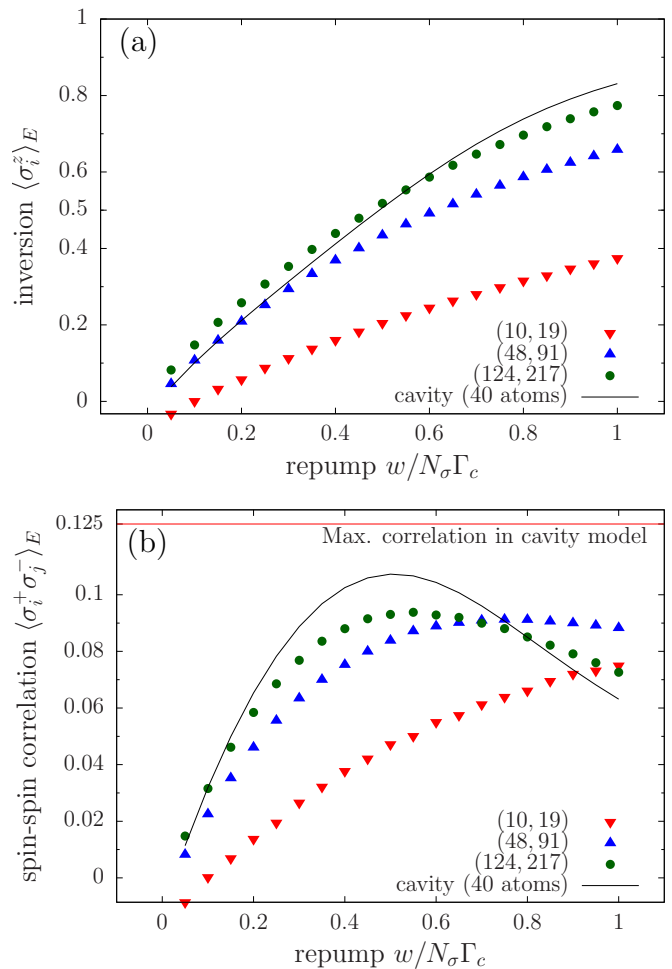


FIG. 5. (color online) Steady-state (a) Inversion and (b) spin-spin correlation as a function of repump strength for three different system sizes (SS) (N_σ, N). The corresponding values for a minimal cavity model with $N_\sigma = 40$ atoms are also plotted. As the system size increases, the inversion and correlation in the ion trap case become similar to the cavity case.

are brought to a uniform superposition of ground and excited states (equator) by applying a $\pi/2$ -pulse about the x -axis. In the frame of the initial laser, the spins then precess around the z -axis at a rate set by the detuning of the laser, for an interrogation period T . Finally, a second $\pi/2$ -pulse rotates the spin about the x -axis and the population is read out using resonance fluorescence. The result is a sinusoidal variation (‘fringe’) of the population, with the amplitude damped by incoherent processes such as spontaneous emission, incoherent repumping and/or dephasing.

Here, after the initial $\pi/2$ -pulse, we intend to allow the σ -spins to interact with the damped set of normal modes during the interrogation period, while continuously repumping the spins incoherently at a rate w [19]. This is achieved by continuous Doppler cooling of the τ ions, and applying Raman and repump beams to the σ -spins, during the interrogation period. Finally, the second $\pi/2$ -

pulse is applied and the population is read out. In the presence of only the repump, the amplitude of the fringe decays at a rate $w/2$. However, the damped COM mode mediates phase-locking of the spins, that leads to a giant collective spin that is robust against individual atom incoherent processes. After a fast initial transient during which the spins phase-lock, the fringe decays at a slower rate; a rate that is set by the phase diffusion of this collective spin. The pair-wise spin-spin interactions ($O(N^2)$ interactions) lead to phase-locking of the spins, while the self interactions of the spins ($O(N)$ interactions) are phase-destroying processes that result in phase diffusion. Figure 6(b) compares the fringe decays for uncorrelated ions and correlated ions. The inset shows the normalized Ramsey fringe amplitude for three different system sizes.

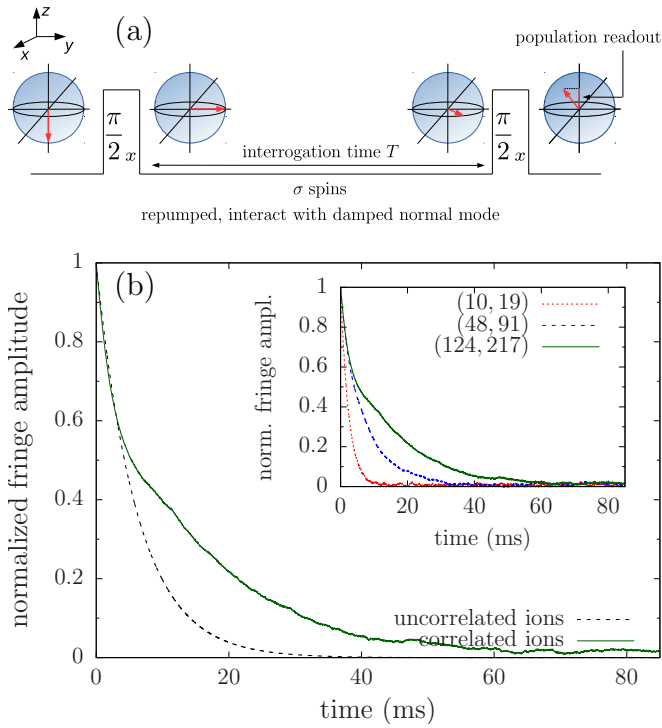


FIG. 6. (color online) (a) Ramsey pulse sequence to probe the collective spin. During the interrogation time, the σ ions interact with a heavily damped normal mode while being continuously repumped. (b) Decay of the Ramsey fringe envelope for uncorrelated ions and a system of correlated ions with SS (124, 217) and $w = N_\sigma \Gamma_c / 2$. Once the σ -spins have phase-locked, the Ramsey fringe decays at a slower rate than when the spins are uncorrelated. Inset: Fringe decay as a function of time for three different system sizes for $w = N_\sigma \Gamma_c / 2$.

Figure 7(a) shows the decay rate of the Ramsey fringe envelope as a function of repump strength for SS (124, 217). The collective spin clearly decays at a slower rate compared to the case when only repumping is present, indicating phase-locking of the spins.

In contrast to simple repumping schemes (Fig. 3), the excited state $|a\rangle$ does not rapidly decay to $|3\rangle$ alone in

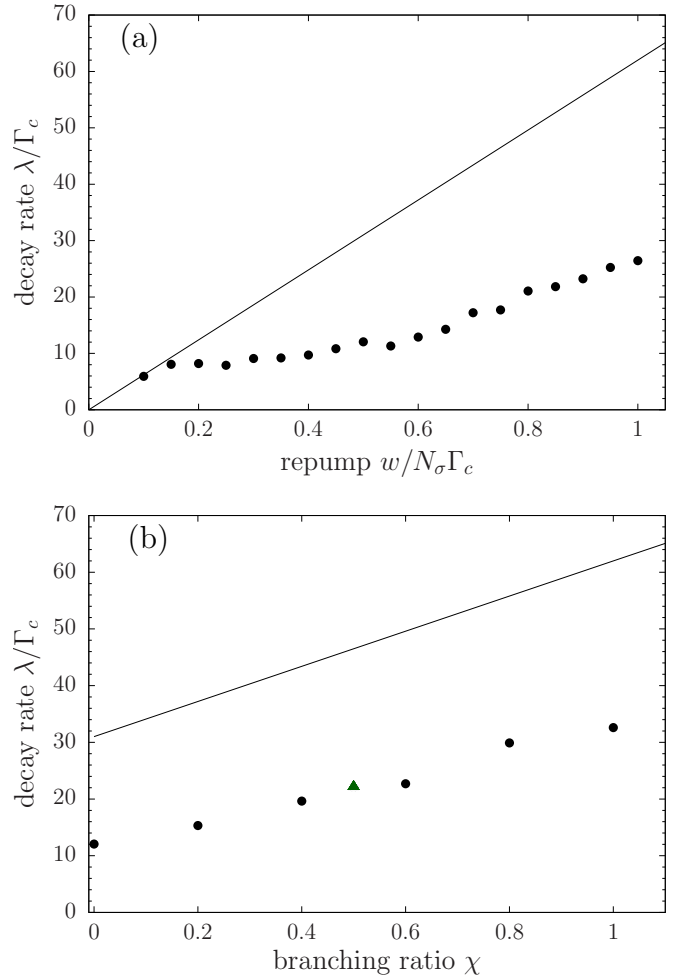


FIG. 7. (color online) (a) Decay rate of the Ramsey fringe envelope (dots) as a function of repump strength for SS (124, 217). The solid line shows the decay rate if only repumping is present. (b) Decay rate of the Ramsey fringe envelope (dots) as a function of the relative branching ratio for SS (124, 217) and $w = N_\sigma \Gamma_c / 2$. The solid line shows the decay rate if only repumping (with branching) is present. The repumping scheme proposed in this paper (see Fig. 4) with the $^{25}\text{Mg}^+$ ions has a relative branching ratio of 0.5, and is indicated by a green triangle.

realistic repumping schemes. A fraction of the population in $|a\rangle$ also decays back to the initial state $|1\rangle$, with a relative branching ratio χ that gives the ratio of population transfer to $|1\rangle$ and $|3\rangle$. The effect of this is to introduce an additional dephasing $\Gamma_w = \chi w$, where w is the repumping strength. This can be accounted for by setting $\Gamma_d \rightarrow \Gamma_d + \Gamma_w$ in the master equation (19). The decay rate for various relative branching ratios is shown in Fig. 7(b) for SS (124, 217) and $w = 0.5 N_\sigma \Gamma_c$. The dephasing due to branching scales with the rate of synchronization, which is set by the repump strength w . Despite this, the phase-locking of the spins still ensures that the fringe amplitude decays slower compared to the situation when only repumping (with branching) is present.

In the cavity model, the plot of decay rate vs repump strength for reasonably large system sizes ($N_\sigma \gtrsim 40$) is approximately the same, when the repump strength is in units of $N_\sigma \Gamma_c$. However, the constant Γ_c is independent of N_σ in the cavity case. In the ion trap system, the spin-spin coupling is predominantly mediated by the single nearly-resonant COM mode, although a total of N modes are available. Hence, the coupling of each spin to the COM mode scales as $1/\sqrt{N}$, and hence Γ_c (see Eq. (21)) decreases as N increases. As a result, when the decay rate is measured in absolute units, say, hertz for example, the decay rate decreases as N increases. This is demonstrated in Fig. 8(a) for SS (i) (48, 91), (ii) (94, 169), and (iii) (124, 217).

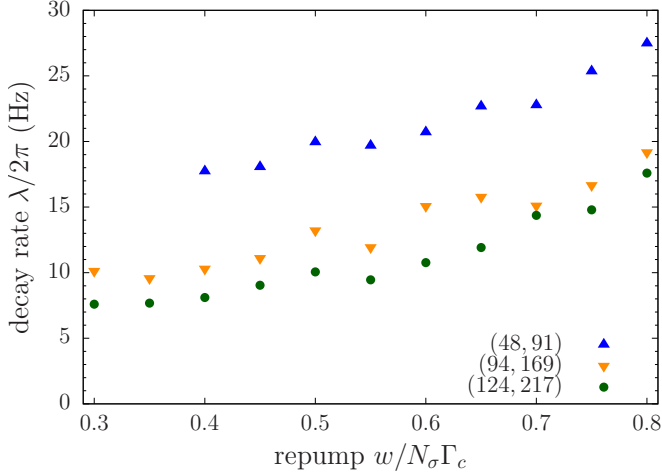


FIG. 8. (color online) Decay rate of the Ramsey fringe envelope (dots) as a function of repump strength for three different system sizes. The fringes persist for longer with increasing N .

The variance of the population measurement at the end of the Ramsey sequence could give information about the spin-spin correlations present in the system. Using J^x, J^y, J^z to denote the components of the collective spin, we note that the variance of the total inversion $(\Delta J^z)^2$ after the second $\pi/2$ -pulse in the Ramsey sequence is just $(\Delta J^y)^2$ before that pulse. Before the second $\pi/2$ -pulse, the variance $(\Delta J^y)^2$ can be expressed as

$$(\Delta J^y)^2 = \frac{N_\sigma}{4} + \frac{N_\sigma(N_\sigma - 1)}{2} (\langle \sigma_i^+ \sigma_j^- \rangle_E - \text{Re} \langle \sigma_i^+ \sigma_j^+ \rangle_E) - N_\sigma^2 (\text{Im} \langle \sigma_i^+ \rangle_E)^2. \quad (22)$$

The quantities $\text{Re} \langle \sigma_i^+ \sigma_j^+ \rangle_E$ and $\text{Im} \langle \sigma_i^+ \rangle_E$ are zero once the fringe envelope has decayed to zero. Thus, the steady-state variance $(\Delta J^z)^2$ ($(\Delta J^y)^2$ before the second $\pi/2$ -pulse) scales as $N_\sigma^2 \langle \sigma_i^+ \sigma_j^- \rangle_E$ ($N_\sigma \gg 1$) giving a measure of the non-zero steady-state spin-spin correlations. Experimentally, this corresponds to a situation where the Ramsey fringe amplitude has decayed to zero but the variance of the population inversion readout is significantly larger (N_σ^2 scaling) than what we would expect

for uncorrelated spins, as shown in Fig. 9. Further, the N_σ^2 scaling shows the all-to-all nature of the spin-spin interactions. The variance could be a measurable quantity even when the repumping has a non-zero relative branching ratio: the inset of Fig. 9 shows the steady-state variance as a function of relative branching ratio for SS (124, 217) and $w = N_\sigma \Gamma_c / 2$.

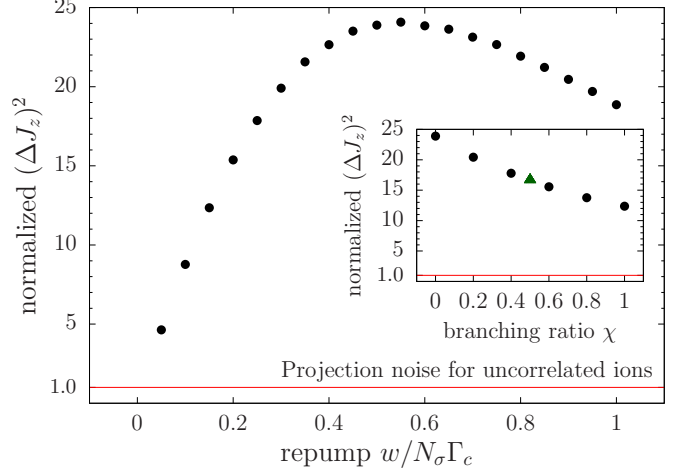


FIG. 9. (color online) Steady-state variance of inversion as a function of repump strength w for SS (124, 217) at the end of the Ramsey pulse sequence, normalized to the projection noise for uncorrelated ions ($N_\sigma/4$). Inset: Normalized steady-state variance of inversion as a function of relative branching ratio χ for SS (124, 217) and $w = N_\sigma \Gamma_c / 2$. The repumping scheme proposed in this paper (see Fig. 4) with the $^{25}\text{Mg}^+$ ions has a relative branching ratio of 0.5, and is indicated by a green triangle.

3. Potential advantage of Sub-Doppler cooling

Our current design uses Doppler cooling to provide a heavily damped COM mode that can mediate spin-spin interactions. In a minimal model, we can ignore the coupling of the spins to all the modes other than the resonant COM mode. Further ignoring spontaneous emission and dephasing, this minimal model is described by the master equation

$$\dot{\mu}_\sigma = \frac{\Gamma_c}{2} (\bar{n}_{\text{COM}} + 1) \mathcal{D}[J^-] \mu_\sigma + \frac{\Gamma_c}{2} \bar{n}_{\text{COM}} \mathcal{D}[J^+] \mu_\sigma + \frac{w}{2} \sum_l \mathcal{D}[\sigma_l^+] \mu_\sigma, \quad (23)$$

where $J^\pm = \sum_l \sigma_l^\pm$ are ladder operators for the collective spin. It is instructive to study the change in the decay rate as \bar{n}_{COM} is changed. We note that this model is invariant under the permutation of spins. We compute exact decay rates of the Ramsey fringes for different values of \bar{n}_{COM} using a numerical method that exploits

the $SU(4)$ symmetry of spin systems that obey permutation symmetry [35]. We summarize these results in Fig. 10(a) for SS (124, 217) and $w = N_\sigma \Gamma_c / 2$. The decay rate can be as low as Γ_c if the COM mode is cooled to $\bar{n}_{\text{COM}} \approx 0$. With Doppler cooling, our model system has $\bar{n}_{\text{COM}} \approx 4.7$, and this gives us a decay rate around $10\Gamma_c$, an order of magnitude higher than what is achievable. Clearly, sub-Doppler cooling techniques [36–39] could be used to observe longer lasting fringes.

Spin synchronization mediated by a sub-Doppler cooled normal mode, and with a repumping scheme that has a negligible relative branching ratio, can improve metrology with ion traps. With uncorrelated ions that have $1/T_1$ (population decay) and $1/T_2$ (dephasing) rates, the Ramsey fringe envelope decays at a rate $\Gamma_s = (T_1^{-1} + T_2^{-1})/2$. However, with synchronized ions, the Ramsey fringe envelope decays slower than in the case of uncorrelated ions in the regime where $\Gamma_c \ll \Gamma_s \ll w$ [19]. The synchronization effect causes the collective spin to be robust against individual ion decoherence processes. This is illustrated in Fig. 10(b) for the minimal model considered in Eq. (23) with $\bar{n}_{\text{COM}} = 0$, and with additional spontaneous emission ($\Gamma_{\text{sp}} = 1/T_1$) and dephasing ($\Gamma_{\text{d}} = 1/T_2$) processes for the individual ions.

IV. CONCLUSION

We have presented and numerically analyzed a model of steady-state spin synchronization in an ion trap, where the synchronization is mediated by a heavily damped normal mode of vibration. This is achieved by mapping the dynamics of cavity steady-state superradiance onto an ion trap system by exploiting the overarching similarity of an optical cavity mode and a normal mode of vibration.

We have considered a model system of two species of ions in a Penning trap, although the present scheme can also be implemented with 1D or 2D RF traps that can trap a mesoscopic number ($\gtrsim 20$) of ions. As the system size increases, the steady-state spin-spin correlations in the ion trap are similar to that in the cavity case, since the effects of a non-zero temperature due to the Doppler cooling are negated.

We have proposed an experimental scheme using a Ramsey pulse sequence that can be used to observe features of the collective spin that develops in the ion trap. The Ramsey fringes persist longer when the spins are synchronized, with a lower decay rate than we expect from the incoherent repumping. Further, the variance of the population readout at the end of the Ramsey sequence scales as $N_\sigma^2 \langle \sigma_i^+ \sigma_j^- \rangle_E$, providing a straightforward means for documenting spin-spin correlation and the all-to-all nature of the coupling. These signatures of spin synchronization persist even when the repumping is imperfect and has a non-zero branching ratio back to the initial state. We also show that the Ramsey fringes decay slower with increasing ion number N since the rate Γ_c de-

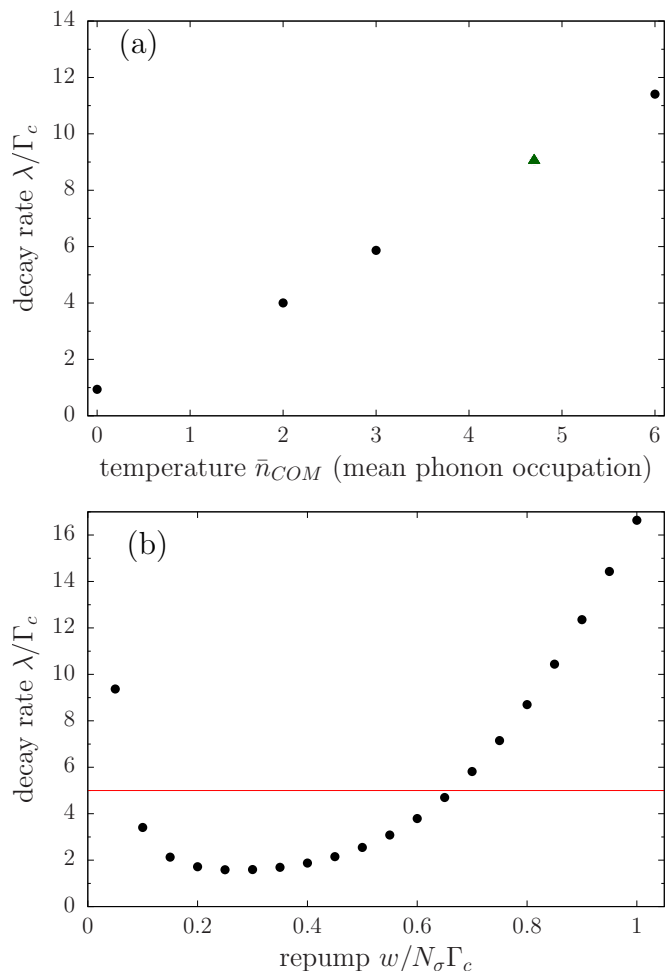


FIG. 10. (color online) (a) Decay rate of the Ramsey fringe envelope as a function of the mean occupation \bar{n}_{COM} of the center-of-mass (COM) mode for $N_\sigma = 124$ ions. The rates shown here are calculated using the $SU(4)$ method for a minimal model of a single mode (COM) interacting with the σ ions (Eq. (23)). The Doppler cooling scheme proposed is shown by a green triangle. (b) Decay rate of the Ramsey fringe envelope as a function of repump strength w for $N_\sigma = 124$ ions. The minimal model of Eq. (23) is used with $\bar{n}_{\text{COM}} = 0$, but with additional spontaneous emission and dephasing processes for the individual ions ($\Gamma_{\text{sp}} = \Gamma_{\text{d}} = 5\Gamma_c$). The decay rate for uncorrelated ions is shown by the horizontal line ($\lambda = 5\Gamma_c$). Synchronization can prolong visibility of Ramsey fringes.

creases with increasing N . In the cavity case, this would be equivalent to a single-atom cooperativity parameter in the superradiant laser that scales inversely with the number of atoms.

We observe that a Ramsey fringe decay rate of around $10\Gamma_c$, achieved with Doppler cooling ($\bar{n}_{\text{COM}} \approx 4.7$), can be as low as $\sim \Gamma_c$ if the ions are cooled to their zero-point motion ($\bar{n}_{\text{COM}} \approx 0$). An ensemble of spins synchronized via this scheme can give fringes that decay slower than what the decay and dephasing processes dictate for uncorrelated spins. This also relies on using a repump scheme that has a negligible branching ratio back to the

initial state.

With this mapping, we can apply the unique tools that ion traps offer to study spin synchronization from steady-state superradiance. The ability to address single ions or specific subsets of ions in a trap can greatly advance studies of synchronization of two ensembles of ions that share the same damped normal mode [40]. Ion traps could be used to explore quantum phase transitions between synchronized and unsynchronized phases, studying the build-up of correlations at the individual spin level. Recently, a cooling scheme for atoms in cavities that takes advantage of the collective interactions via a damped cavity mode has been proposed [41]. It will be interesting to see if there are analogies to this ‘supercooling’ in ion trap systems.

ACKNOWLEDGMENTS

The authors acknowledge helpful discussions with Martin Gärttner, Yiheng Lin and Peiru He. This work is supported by the National Science Foundation under Grants PHY-1521080, PHY-1404263 and PHY-1125844, and by DARPA. This manuscript is the contribution of NIST and is not subject to US copyright.

Appendix A: Damping of the normal modes

For brevity, we will use the notation $\rho \equiv \rho_{\tau, \text{ph}}$ and $\mu \equiv \mu_{\text{ph}}$ in this section.

In the Lamb-Dicke regime ($\langle (kz_m)^2 \rangle^{1/2} \ll 1$), we can expand the RHS of the master equation (1) in powers of $\{\eta_n^\tau\}$. Up to second order in $\{\eta_n^\tau\}$ we get

$$\dot{\rho} = (\mathcal{L}_S + \mathcal{L}_R + \mathcal{L}_{SR})\rho, \quad (\text{A1})$$

where

$$\begin{aligned} \mathcal{L}_S \rho &= -i \left[\sum_n \omega_n b_n^\dagger b_n, \rho \right], \\ \mathcal{L}_R \rho &= -i \left[-\frac{1}{2} \Delta_\tau \sum_m \tau_m^z, \rho \right] + \frac{\Gamma}{2} \sum_m \mathcal{D}[\tau_m^-] \rho, \text{ and} \\ \mathcal{L}_{SR} \rho &= \mathcal{L}_{SR}^{(1)} \rho + \mathcal{L}_{SR}^{(2)} \rho, \end{aligned} \quad (\text{A2})$$

with

$$\begin{aligned} \mathcal{L}_{SR}^{(1)} \rho &= -i \left[\frac{\Omega_\tau}{2} \sum_m (kz_m) (\tau_m^- + \tau_m^+), \rho \right], \text{ and} \\ \mathcal{L}_{SR}^{(2)} \rho &= \frac{\Gamma_\tau}{2} \langle u^2 \rangle \sum_m \tau_m^- (2(kz_m) \rho(kz_m) \\ &\quad - (kz_m)^2 \rho - \rho(kz_m)^2) \tau_m^+. \end{aligned} \quad (\text{A3})$$

Here S denotes the system of normal modes, and R denotes the reservoir of τ ions.

We first transform to an interaction picture with $\mathcal{L}_0 = \mathcal{L}_S + \mathcal{L}_R$ [42]. We then have

$$\dot{\tilde{\rho}} = \tilde{\mathcal{L}}_{SR} \tilde{\rho} = (\tilde{\mathcal{L}}_{SR}^{(1)} + \tilde{\mathcal{L}}_{SR}^{(2)}) \tilde{\rho}, \quad (\text{A4})$$

where $\tilde{\rho} = e^{-(\mathcal{L}_S + \mathcal{L}_R)t} \rho$ and $\tilde{\mathcal{L}}_{SR} = e^{-(\mathcal{L}_S + \mathcal{L}_R)t} \mathcal{L}_{SR} e^{(\mathcal{L}_S + \mathcal{L}_R)t}$. Integrating Eq. (A4) and substituting the formal solution of $\tilde{\rho}(t)$ back into Eq. (A4) gives (up to second order in $\{\eta_n^\tau\}$),

$$\dot{\tilde{\rho}} = \tilde{\mathcal{L}}_{SR}^{(1)} \tilde{\rho}(0) + \tilde{\mathcal{L}}_{SR}^{(2)} \tilde{\rho}(0) + \int_0^t dt' \tilde{\mathcal{L}}_{SR}^{(1)}(t) \tilde{\mathcal{L}}_{SR}^{(1)}(t') \tilde{\rho}(t'). \quad (\text{A5})$$

When the couplings $\{\Omega_\tau \eta_n^\tau\} \ll \Gamma_\tau$, the τ ions serve as a reservoir of ions in a steady-state dictated by the reservoir Liouvillian \mathcal{L}_R . In this case, the steady-state R_0 is the ground state of the τ ions, i.e., $R_0 = |g\rangle \langle g|^{\otimes N_\tau}$. Starting from an initial uncorrelated state $\tilde{\rho}(0) = \tilde{\mu}(0) R_0$, we then use a decorrelation approximation to write $\tilde{\rho}(t) \approx \tilde{\mu}(t) R_0$ for subsequent times, and trace out the spin degrees of freedom of the τ ions:

$$\begin{aligned} \dot{\tilde{\mu}} &= \text{Tr}_R [\tilde{\mathcal{L}}_{SR}^{(1)}(t) \tilde{\mu}(0) R_0] + \text{Tr}_R [\tilde{\mathcal{L}}_{SR}^{(2)}(t) \tilde{\mu}(0) R_0] \\ &\quad + \int_0^t dt' \text{Tr}_R [\tilde{\mathcal{L}}_{SR}^{(1)}(t) \tilde{\mathcal{L}}_{SR}^{(1)}(t') \tilde{\mu}(t') R_0]. \end{aligned} \quad (\text{A6})$$

The first term vanishes because $\langle \tau_m^\pm \rangle = 0$ in the ground state, and the second term vanishes because $\langle \tau_m^+ \tau_m^- \rangle$ is zero in the ground state.

The structure of $\mathcal{L}_{SR}^{(1)}$ (Eq. (A2)) suggests that we need to find the time evolution of the superoperators $\tilde{\tau}_m^\pm \otimes I$ and $I \otimes (\tilde{\tau}_m^\mp)^T$.

This notation for a superoperator is to be understood as follows. Let A, B be two operators acting on a Hilbert space spanned by $|e\rangle, |g\rangle$. Then the action of a superoperator $\mathcal{L} = A \otimes (B)^T$ on a vector in the corresponding Liouville space, for eg. $|\lambda\rangle\rangle = |e\rangle \langle g|$ is $\mathcal{L}|\lambda\rangle\rangle = A|e\rangle \langle g| B$.

From $\tilde{\mathcal{L}}_I = e^{-(\mathcal{L}_S + \mathcal{L}_R)t} \mathcal{L}_I e^{(\mathcal{L}_S + \mathcal{L}_R)t}$, we have,

$$\dot{\tilde{\mathcal{L}}}_I = [\tilde{\mathcal{L}}_I, \mathcal{L}_R]. \quad (\text{A7})$$

This immediately gives the following complete set of equations:

$$\begin{aligned} \frac{d}{dt} \tilde{\tau}_m^- \otimes I &= -\left(\frac{\Gamma_\tau}{2} - i\Delta_\tau\right) \tilde{\tau}_m^- \otimes I, \\ \frac{d}{dt} \tilde{\tau}_m^+ \otimes I &= \left(\frac{\Gamma_\tau}{2} - i\Delta_\tau\right) \tilde{\tau}_m^+ \otimes I + \Gamma_\tau \tilde{\tau}_m^z \otimes (\tilde{\tau}_m^+)^T, \\ \frac{d}{dt} \tilde{\tau}_m^z \otimes I &= -2\Gamma_\tau \tilde{\tau}_m^- \otimes (\tilde{\tau}_m^+)^T. \end{aligned} \quad (\text{A8})$$

The time evolution of the superoperators is then given by

$$\begin{aligned}
\tilde{\tau}_m^- \otimes I(t) &= \tau_m^- \otimes I e^{-(\frac{\Gamma_\tau}{2} - i\Delta_\tau)t}, \\
\tilde{\tau}_m^+ \otimes I(t) &= \tau_m^+ \otimes I e^{(\frac{\Gamma_\tau}{2} - i\Delta_\tau)t} + \tau_m^z \otimes (\tau_m^+)^T \times \\
&\quad \left(e^{(\frac{\Gamma_\tau}{2} - i\Delta_\tau)t} - e^{-(\frac{\Gamma_\tau}{2} + i\Delta_\tau)t} \right). \quad (\text{A9})
\end{aligned}$$

Hermitian conjugation of the above two equations gives the time evolution of the other two superoperators.

The master equation can then be written as

$$\begin{aligned}
\dot{\tilde{\mu}} = & \\
& - \sum_m \sum_n \sum_k \left(\frac{\Omega_\tau}{2} \eta_n^\tau \mathcal{M}_{mn} \right) \left(\frac{\Omega_\tau}{2} \eta_k^\tau \mathcal{M}_{mk} \right) \times \int_0^t dt' \left[\right. \\
& \left\{ \tilde{b}_n(t) + \tilde{b}_n^\dagger(t) \right\} \left\{ \tilde{b}_k(t') + \tilde{b}_k^\dagger(t') \right\} \tilde{\mu}(t') e^{-(\frac{\Gamma_\tau}{2} - i\Delta_\tau)(t-t')} \\
& - \left\{ \tilde{b}_n(t) + \tilde{b}_n^\dagger(t) \right\} \tilde{\mu}(t') \left\{ \tilde{b}_k(t') + \tilde{b}_k^\dagger(t') \right\} e^{-(\frac{\Gamma_\tau}{2} + i\Delta_\tau)(t-t')} \\
& - \left\{ \tilde{b}_k(t') + \tilde{b}_k^\dagger(t') \right\} \tilde{\mu}(t') \left\{ \tilde{b}_n(t) + \tilde{b}_n^\dagger(t) \right\} e^{-(\frac{\Gamma_\tau}{2} - i\Delta_\tau)(t-t')} \\
& \left. + \tilde{\mu}(t') \left\{ \tilde{b}_k(t') + \tilde{b}_k^\dagger(t') \right\} \left\{ \tilde{b}_n(t) + \tilde{b}_n^\dagger(t) \right\} e^{-(\frac{\Gamma_\tau}{2} + i\Delta_\tau)(t-t')} \right]. \quad (\text{A10})
\end{aligned}$$

The time evolution of the mode annihilation and creation operators is given by $\tilde{b}_n(t) = b_n e^{-i\omega_n t}$ and $\tilde{b}_n^\dagger(t) = b_n^\dagger e^{i\omega_n t}$.

If $\tilde{\mu}(t')$ doesn't change significantly on the timescale Γ_τ^{-1} for the decay of correlations in the reservoir of τ -spins, we can perform a Markov approximation and set $\tilde{\mu}(t') \approx \tilde{\mu}(t)$ in Eq. (A10). This is reasonable since the damping rates of the normal modes are of the order of $\frac{(\Omega_\tau \eta_n^\tau)^2}{\Gamma_\tau}$, and for laser intensities such that $\Omega_\tau \eta_n^\tau \ll \Gamma_\tau$, this implies $\frac{(\Omega_\tau \eta_n^\tau)^2}{\Gamma_\tau} \ll \Gamma_\tau$. Further, we can extend the upper limit of the integration to ∞ since for significant evolution of $\mu(t)$, we are interested in $t \gg \Gamma_\tau^{-1}$.

After performing the integration over $\chi = t - t'$ in Eq. (A10), we encounter terms rotating with frequencies $\omega_n + \omega_k$ and $\omega_n - \omega_k$. The former terms are rapidly oscillating, and can be dropped.

Performing the reverse transformation $\mu = e^{\mathcal{L}st} \tilde{\mu}$ gives us the master equation for the damping of the normal modes, which accounts for the coupling between the modes as well:

$$\begin{aligned}
\frac{d}{dt} \mu = & -i \left[\sum_n \omega_n' b_n^\dagger b_n, \mu \right] \\
& + \sum_n D_{n,n}^- (2b_n \mu b_n^\dagger - b_n^\dagger b_n \mu - \mu b_n^\dagger b_n) \\
& + \sum_n D_{n,n}^+ (2b_n^\dagger \mu b_n - b_n b_n^\dagger \mu - \mu b_n b_n^\dagger) \\
& -i \sum_{n \neq k} C_{k,n}^- (b_n \mu b_k^\dagger - b_k \mu b_n^\dagger + b_n^\dagger b_k \mu - \mu b_k^\dagger b_n) \\
& -i \sum_{n \neq k} C_{k,n}^+ (b_n^\dagger \mu b_k - b_k^\dagger \mu b_n + b_n b_k^\dagger \mu - \mu b_k b_n^\dagger) \\
& \sum_{n \neq k} D_{k,n}^- (b_n \mu b_k^\dagger + b_k \mu b_n^\dagger - b_n^\dagger b_k \mu - \mu b_k^\dagger b_n) \\
& \sum_{n \neq k} D_{k,n}^+ (b_n^\dagger \mu b_k + b_k^\dagger \mu b_n - b_n b_k^\dagger \mu - \mu b_k b_n^\dagger). \quad (\text{A11})
\end{aligned}$$

Here the coefficients are given by

$$\begin{aligned}
\omega_n' &= \omega_n + R_{n,n}^- (\Delta_\tau + \omega_n) + R_{n,n}^+ (\Delta_\tau - \omega_n), \\
C_{k,n}^\pm &= R_{k,n}^\pm (\Delta_\tau \mp \omega_k), \\
D_{k,n}^\pm &= R_{k,n}^\pm \frac{\Gamma_\tau}{2}, \text{ where} \\
R_{k,n}^\pm &= \frac{\sum_m (\frac{1}{2} \Omega_\tau \eta_m^\tau \mathcal{M}_{mn}) (\frac{1}{2} \Omega_\tau \eta_k^\tau \mathcal{M}_{mk})}{\frac{\Gamma_\tau^2}{4} + (\Delta_\tau \mp \omega_n)^2}. \quad (\text{A12})
\end{aligned}$$

The Doppler cooling introduces couplings between the different modes, with the coupling strengths between two modes decreasing as their frequency separation increases. The result of such mode cross-coupling is to introduce an admixture of other modes into the mode of interest, which in the example we consider is the highest frequency center-of-mass (COM) mode. The symmetric coupling of the COM mode to the ions then deteriorates, but the essential physics still remains the same. The situation is analogous to introducing a random component in the positions of atoms relative to the cavity standing wave in the superradiant laser. For simplicity, we assume these mode cross-couplings to be small and neglect them, use $D_n^\pm \equiv D_{n,n}^\pm$, $R_n^\pm \equiv R_{n,n}^\pm$ to simplify the notation, and arrive at the master equation describing the damping of individual normal modes (Eq. (4)).

Appendix B: Schrieffer-Wolff formalism for the three-level σ ions

The idea is to work in operator space, i.e. in the vector space S spanned by the vectors $|1\rangle \langle 1|, |1\rangle \langle 2|, \dots, |3\rangle \langle 3|$. The Liouvillian describing the dynamics can be written as the sum of a zeroth order Liouvillian \mathcal{L}_0 and a perturbation \mathcal{V} . Based on the eigenvalues $\{\lambda_i\}$ of \mathcal{L}_0 , the space

S can be partitioned into a slow subspace, spanned by eigenvectors with eigenvalue 0, and a complementary fast subspace spanned by eigenvectors with non-zero eigenvalue [26]. If the left and right eigenvectors associated with an eigenvalue λ_i are $\langle\langle l_i|$ and $|r_i\rangle\rangle$ respectively, the projectors P and Q onto the slow and fast subspaces are

$$\begin{aligned} P &= \sum_{i:\{\lambda_i\}=0} |r_i\rangle\rangle\langle\langle l_i|, \\ Q &= 1 - P = \sum_{i:\{\lambda_i\}\neq 0} |r_i\rangle\rangle\langle\langle l_i|. \end{aligned} \quad (\text{B1})$$

Any superoperator $A : S \rightarrow S$ can now be represented as

$$A = \begin{pmatrix} A^P & A^- \\ A^+ & A^Q \end{pmatrix} = \begin{pmatrix} PAP & PAQ \\ QAP & QAQ \end{pmatrix}. \quad (\text{B2})$$

The perturbation \mathcal{V} in general couples the slow and fast subspaces. The Schrieffer-Wolff formalism provides a systematic, order-by-order procedure to find the effective Liouvillian \mathcal{L}^{eff} in the slow subspace that arises from this coupling. Explicitly, at the first three orders of perturbation theory,

$$\begin{aligned} \mathcal{L}_1^{\text{eff}} &= \mathcal{V}^P \\ \mathcal{L}_2^{\text{eff}} &= -\mathcal{V}^- \mathcal{L}_0^{-1} \mathcal{V}^+ \\ \mathcal{L}_3^{\text{eff}} &= \mathcal{V}^- \mathcal{L}_0^{-1} \mathcal{V}^Q \mathcal{L}_0^{-1} \mathcal{V}^+ - \frac{1}{2} \{ \mathcal{V}^P, \mathcal{V}^- \mathcal{L}_0^{-2} \mathcal{V}^+ \}_+, \end{aligned} \quad (\text{B3})$$

$$\begin{aligned} \mathcal{V} &= \begin{pmatrix} \mathcal{V}^P & \mathcal{V}^- \\ \mathcal{V}^+ & \mathcal{V}^Q \end{pmatrix} \\ &= \begin{pmatrix} 0 & 0 & \Gamma_1 & 0 & 0 & i\frac{g_1}{2} & -i\frac{g_1^*}{2} & 0 & 0 \\ 0 & -i(\Delta_1 - \Delta_2) & 0 & 0 & 0 & i\frac{g_2}{2} & 0 & -i\frac{g_2^*}{2} & 0 \\ 0 & 0 & -(\Gamma_1 + \Gamma_2) & 0 & 0 & -i\frac{g_1}{2} & i\frac{g_1^*}{2} & i\frac{g_2}{2} & -i\frac{g_2^*}{2} \\ 0 & 0 & 0 & i(\Delta_1 - \Delta_2) & 0 & 0 & -i\frac{g_2}{2} & 0 & i\frac{g_2^*}{2} \\ 0 & 0 & \Gamma_2 & 0 & 0 & 0 & 0 & -i\frac{g_2^*}{2} & i\frac{g_2}{2} \\ \hline i\frac{g_1^*}{2} & i\frac{g_2^*}{2} & -i\frac{g_1}{2} & 0 & 0 & -\frac{\Gamma_1 + \Gamma_2}{2} & 0 & 0 & 0 \\ -i\frac{g_1}{2} & 0 & i\frac{g_1^*}{2} & -i\frac{g_2^*}{2} & 0 & 0 & -\frac{\Gamma_1 + \Gamma_2}{2} & 0 & 0 \\ 0 & -i\frac{g_1}{2} & i\frac{g_2}{2} & 0 & -i\frac{g_2^*}{2} & 0 & 0 & -\frac{\Gamma_1 + \Gamma_2}{2} & 0 \\ 0 & 0 & -i\frac{g_2^*}{2} & i\frac{g_1^*}{2} & i\frac{g_2}{2} & 0 & 0 & 0 & -\frac{\Gamma_1 + \Gamma_2}{2} \end{pmatrix}. \end{aligned} \quad (\text{B4})$$

The matrix has been partitioned to show the various blocks that make up the perturbation. Using Eq. (B3), we calculate $\mathcal{L}^{\text{eff}} = \mathcal{L}_1^{\text{eff}} + \mathcal{L}_2^{\text{eff}} + \mathcal{L}_3^{\text{eff}}$, which is the effective

where $\{A, B\}_+ = AB + BA$.

Table III gives the notation we adopt for the basis vectors in S . We split the superoperator appearing in Eq. (8) into a zeroth order Liouvillian \mathcal{L}_0 and a perturbation \mathcal{V} . \mathcal{L}_0 is already diagonal in the chosen basis. The third column of Table III gives the eigenvalues associated with \mathcal{L}_0 for each of the basis. Then, the subspace spanned by the eigenvectors with eigenvalue 0, i.e. $\{|A_1\rangle\rangle, |A_3\rangle\rangle, |A_5\rangle\rangle, |A_7\rangle\rangle, |A_9\rangle\rangle\}$ is the slow subspace.

TABLE III. Basis vectors in operator space S . The chosen zeroth order Liouvillian \mathcal{L}_0 is diagonal in the above basis. The eigenvalues of \mathcal{L}_0 are given in the third column.

Notation	Basis	Eigenvalue
$ A_1\rangle\rangle$	$ 1\rangle\langle 1 $	0
$ A_2\rangle\rangle$	$ 1\rangle\langle 2 $	$-i\Delta_1$
$ A_3\rangle\rangle$	$ 1\rangle\langle 3 $	0
$ A_4\rangle\rangle$	$ 2\rangle\langle 1 $	$i\Delta_1$
$ A_5\rangle\rangle$	$ 2\rangle\langle 2 $	0
$ A_6\rangle\rangle$	$ 2\rangle\langle 3 $	$i\Delta_2$
$ A_7\rangle\rangle$	$ 3\rangle\langle 1 $	0
$ A_8\rangle\rangle$	$ 3\rangle\langle 2 $	$-i\Delta_2$
$ A_9\rangle\rangle$	$ 3\rangle\langle 3 $	0

We also write the perturbation \mathcal{V} explicitly as a matrix acting on S . A better insight is obtained if we write vectors and matrices in the following order of basis vectors: $|A_1\rangle\rangle, |A_3\rangle\rangle, \dots, |A_9\rangle\rangle, |A_2\rangle\rangle, \dots, |A_8\rangle\rangle$. In this representation, \mathcal{V} is given by

Liouvillian in the slow subspace. In terms of the symbols defined in Table I, the effective Liouvillian \mathcal{L}^{eff} , correct up to $O(\frac{|g_{1,2}|^2}{\Delta^2})$ is given by,

$$\left(\begin{array}{ccccc} -\Gamma_{13} & i\frac{\Omega_R}{2} + \frac{\Gamma_{1,\times} - \Gamma_{3,\times}}{2} & \Gamma_1 - 2\Gamma_{11} - \Gamma_{31} & -i\frac{\Omega_R^*}{2} + \frac{\Gamma_{1,\times}^* - \Gamma_{3,\times}^*}{2} & \Gamma_{31} \\ i\frac{\Omega_R^*}{2} - \frac{\Gamma_{1,\times}^* + \Gamma_{3,\times}^*}{2} & -i\delta_R - \frac{\Gamma_{13} + \Gamma_{31} + \Gamma_{11} + \Gamma_{33}}{2} & -\frac{\Gamma_{1,\times}^* + \Gamma_{3,\times}^*}{2} & 0 & -i\frac{\Omega_R^*}{2} - \frac{\Gamma_{1,\times}^* + \Gamma_{3,\times}^*}{2} \\ 0 & 0 & -(\Gamma_1 + \Gamma_2) + 2\Gamma_{11} + \Gamma_{13} & 0 & 0 \\ -i\frac{\Omega_R}{2} - \frac{\Gamma_{1,\times} + \Gamma_{3,\times}}{2} & 0 & +\Gamma_{31} + 2\Gamma_{33} & 0 & 0 \\ \Gamma_{13} & -i\frac{\Omega_R}{2} - \frac{\Gamma_{1,\times} - \Gamma_{3,\times}}{2} & -\frac{\Gamma_{1,\times} + \Gamma_{3,\times}}{2} & i\delta_R - \frac{\Gamma_{13} + \Gamma_{31} + \Gamma_{11} + \Gamma_{33}}{2} & i\frac{\Omega_R}{2} - \frac{\Gamma_{1,\times} + \Gamma_{3,\times}}{2} \\ \Gamma_{13} & -i\frac{\Omega_R}{2} - \frac{\Gamma_{1,\times} - \Gamma_{3,\times}}{2} & \Gamma_2 - \Gamma_{13} - 2\Gamma_{33} & i\frac{\Omega_R^*}{2} - \frac{\Gamma_{1,\times}^* - \Gamma_{3,\times}^*}{2} & -\Gamma_{31} \end{array} \right). \quad (\text{B5})$$

Here, the quantities $\Gamma_{1,\times} = \Gamma_1 \frac{g_1 g_2^*}{4\Delta^2}$ and $\Gamma_{3,\times} = \Gamma_2 \frac{g_1 g_2^*}{4\Delta^2}$. The master equation for the σ ion in the slow space is then $\dot{\mu} = \mathcal{L}^{\text{eff}}\mu$, and this is given in Eq. (10) for a collection of σ ions.

There are two points of note here. Firstly, if the system starts within the $|1\rangle, |3\rangle$ manifold spanned by $|A_1\rangle, |A_3\rangle, |A_7\rangle$ and $|A_9\rangle$, then it stays within that manifold. Then we do not need to consider the $|A_5\rangle$ state. Secondly, the terms proportional to $\Gamma_{1,\times}$ and $\Gamma_{3,\times}$ give rise to certain cross-terms. A typical cross-term in the master equation appears as

$$\frac{\Gamma_{1,\times}}{2} (-\sigma^+ \mu - \sigma^z \mu \sigma^+). \quad (\text{B6})$$

We intend to couple the effective two-level system formed by the σ ions to their external motion by tuning the Raman lasers to the red vibrational sideband. In that case, the only significant contributions to ion l from a term such as (B6) will be of the approximate form

$$\frac{1}{2} \frac{\Gamma_1}{\Delta} \sum_n \mathcal{F}_{ln} \sigma_l^+ b_n \mu. \quad (\text{B7})$$

The spin-motion coupling strength in this term is a factor of $\frac{\Gamma}{\Delta}$ smaller than the coherent spin-motion coupling present in the Hamiltonian terms. Subsequently, when we treat the spin-motion coupling perturbatively in comparison with the damping of the normal modes, the contribution from these cross-terms will be $\frac{\Gamma^2}{\Delta^2}$ smaller than the contribution from the Hamiltonian terms. Hence we neglect these cross-terms while writing down Eq. (10).

Appendix C: Effective spin-spin model: Interaction of σ -spins with damped normal modes

We will use the notation $\mu \equiv \mu_\sigma$ in this section. Starting with Eq. (18), we first transform to an interaction picture with $\mathcal{L}_0 = \mathcal{L}_R$. Following the steps outlined in the beginning of Appendix A, we arrive at the following integro-differential equation for the reduced density matrix $\mu(t)$ describing the σ -spins only:

$$\begin{aligned} \dot{\mu}(t) = & \text{Tr}_R[\tilde{\mathcal{L}}_{SR}(t)\mu(0)R_0] \\ & + \int_0^t dt' \text{Tr}_R[\tilde{\mathcal{L}}_{SR}(t)\tilde{\mathcal{L}}_{SR}(t')\mu(t')R_0]. \quad (\text{C1}) \end{aligned}$$

Here, we have used a decorrelation approximation to write $\tilde{\rho}(t) \approx \mu(t)R_0$, where R_0 is the steady-state density matrix for the normal modes under the action of \mathcal{L}_R . Once again, we start from an initial uncorrelated state: $\rho(0) = \mu(0)R_0$. Note that the density matrix $\mu(t)$ and the σ -spin operators do not have overhead tilde (\sim) in this Appendix since $\mathcal{L}_S = 0$ in the present case.

Under the action of \mathcal{L}_R , the steady-state density matrices of each of the normal modes are thermal states. The first term on the RHS of Eq. (C1) vanishes, since the expectation values $\langle b_n \rangle, \langle b_n^\dagger \rangle$ are zero in a thermal state. In order to evaluate the second term, we need to find the time evolution of the superoperators $\tilde{b}_n \otimes I, \tilde{b}_n^\dagger \otimes I, I \otimes (\tilde{b}_n)^T$ and $I \otimes (\tilde{b}_n^\dagger)^T$. Following the lines of the procedure we adopted in finding the time evolution of the superoperators $\tilde{\tau}_m^- \otimes I$, etc. in Appendix A, we get,

$$\begin{aligned} \frac{d}{dt} \tilde{b}_n \otimes I(t) = & - \left(\frac{\kappa_n}{2} (1 + 2\bar{n}_n) + i\tilde{\delta}_n \right) \tilde{b}_n \otimes I \\ & + \kappa_n \bar{n}_n I \otimes (\tilde{b}_n)^T, \\ \frac{d}{dt} I \otimes (\tilde{b}_n)^T = & \left(\frac{\kappa_n}{2} (1 + 2\bar{n}_n) - i\tilde{\delta}_n \right) I \otimes (\tilde{b}_n)^T \\ & - \kappa_n (1 + \bar{n}_n) \tilde{b}_n \otimes I. \quad (\text{C2}) \end{aligned}$$

Solving the above pair of coupled differential equations, we get,

$$\begin{aligned} \tilde{b}_n \otimes I(t) = & \bar{n}_n (I \otimes (b_n)^T - b_n \otimes I) e^{(\frac{\kappa_n}{2} - i\tilde{\delta}_n)t} \\ & + ((1 + \bar{n}_n) b_n \otimes I - \bar{n}_n I \otimes (b_n)^T) e^{-(\frac{\kappa_n}{2} + i\tilde{\delta}_n)t}, \\ I \otimes (\tilde{b}_n)^T(t) = & (1 + \bar{n}_n) (I \otimes (b_n)^T - b_n \otimes I) e^{(\frac{\kappa_n}{2} - i\tilde{\delta}_n)t} \\ & + ((1 + \bar{n}_n) b_n \otimes I - \bar{n}_n I \otimes (b_n)^T) e^{-(\frac{\kappa_n}{2} + i\tilde{\delta}_n)t}. \quad (\text{C3}) \end{aligned}$$

Hermitian conjugation of the above two equations gives the time evolution of $I \otimes (\tilde{b}_n^\dagger)^T$ and $\tilde{b}_n^\dagger \otimes I$. Using the fact that $\langle b_n^\dagger b_n \rangle = \bar{n}_n$, we can now perform the trace over the reservoir of normal modes in Eq. (C1) to arrive at an expression involving intergrals over the σ -spin operators, $\mu(t')$ and complex exponentials. As an example, we consider one of the terms that occur in this expression:

$$-\sum_{l,m,n} \mathcal{F}_{ln} \mathcal{F}_{mn}^* (1 + \bar{n}_n) \int_0^t dt' \sigma_l^\dagger \sigma_m^- \mu(t') e^{-\left(\frac{\kappa_n}{2} + i\delta_n\right)(t-t')}. \quad (\text{C4})$$

We perform a Markov approximation by setting $\mu(t') \approx \mu(t)$. For significant evolution of $\mu(t)$, we are interested in evolution over times that are large compared to the timescales of the reservoir correlations. Only the upper limit of integration in terms like C4 contribute in this coarse-graining procedure.

We then evaluate the simple time integrals over complex exponentials and group the coherent and dissipative parts separately. We then account for the incoherent Raman processes and the incoherent repumping, and arrive at the effective spin-spin model described by the master equation (19), which is the starting point for our numerical analysis.

A note on the validity of approximations: To stop at second-order in perturbation theory, the timescale for the system-reservoir interaction must be long compared to the reservoir correlation time [43]. Further, the Markov approximation requires that the timescale for significant evolution of the system T_S is long compared to the reservoir correlation time. In a minimal model where the spin-spin interactions are mediated only by the COM mode and the other modes are neglected, the perturbation strength and fastest timescale for the σ -spins are determined by the collectively-enhanced spontaneous emission rate, given by $N_\sigma \Gamma_{\text{COM}} (1 + \bar{n}_{\text{COM}})$, where $\Gamma_{\text{COM}} = \mathcal{F}_{\text{COM}}^2 / \kappa_{\text{COM}}$. Since the correlation time for the COM mode is set by κ_{COM} , we require $\kappa_{\text{COM}} \gg N_\sigma \Gamma_{\text{COM}} (1 + \bar{n}_{\text{COM}}) \gtrsim T_S$ for second-order perturbation theory and the Markov approximation to be valid.

Appendix D: Numerical simulation using c -number Langevin equations

We start by writing the quantum Langevin equations (QLE) for the spin operators σ_i^x , σ_i^y and σ_i^z for a spin i from the master equation (19):

$$\begin{aligned} \frac{d}{dt} \sigma_i^x &= D_i^x + F_i^x \\ &= - \left\{ \Gamma_{ii}^- + \Gamma_{ii}^+ + \frac{\Gamma_{31}}{2} + \frac{\Gamma_{13} + w}{2} + \frac{\Gamma_d}{2} \right\} \sigma_i^x \\ &\quad - B_i \sigma_i^y + \sum_{j \neq i} (\Gamma_{ji}^- - \Gamma_{ji}^+) \sigma_i^z \sigma_j^x \\ &\quad + \sum_{j \neq i} J_{ji} \sigma_i^z \sigma_j^y + F_i^x, \\ \frac{d}{dt} \sigma_i^y &= D_i^y + F_i^y \\ &= - \left\{ \Gamma_{ii}^- + \Gamma_{ii}^+ + \frac{\Gamma_{31}}{2} + \frac{\Gamma_{13} + w}{2} + \frac{\Gamma_d}{2} \right\} \sigma_i^y \\ &\quad + B_i \sigma_i^x + \sum_{j \neq i} (\Gamma_{ji}^- - \Gamma_{ji}^+) \sigma_i^z \sigma_j^y \\ &\quad - \sum_{j \neq i} J_{ji} \sigma_i^z \sigma_j^x + F_i^y, \\ \frac{d}{dt} \sigma_i^z &= D_i^z + F_i^z \\ &= - \left\{ 2(\Gamma_{ii}^- + \Gamma_{ii}^+) + \Gamma_{31} + \Gamma_{13} + w \right\} \sigma_i^z \\ &\quad + \left\{ \Gamma_{13} + w - (2(\Gamma_{ii}^- - \Gamma_{ii}^+) + \Gamma_{31}) \right\} \\ &\quad - \sum_{j \neq i} (\Gamma_{ji}^- - \Gamma_{ji}^+) (\sigma_i^x \sigma_j^x + \sigma_i^y \sigma_j^y) \\ &\quad - \sum_{j \neq i} J_{ji} (\sigma_i^x \sigma_j^y - \sigma_i^y \sigma_j^x) + F_i^z. \end{aligned} \quad (\text{D1})$$

Here, F_i^x , F_i^y and F_i^z are operators that account for the noise because of coupling to an external environment. These noise operators are correlated according to

$$\langle F_i^\mu(t) F_j^\nu(t') \rangle = 2 \langle D_{ij}^{\mu\nu} \rangle \delta(t - t'), \quad (\text{D2})$$

where $\mu, \nu = x, y, z$ and i, j are the spin indices. The generalized Einstein relation [33] can be used to determine the correlation matrix elements $2 \langle D_{ij}^{\mu\nu} \rangle$:

$$2 \langle D_{ij}^{\mu\nu} \rangle = - \langle \sigma_\mu^i D_\nu^j \rangle - \langle D_\mu^i \sigma_\nu^j \rangle + \frac{d}{dt} \langle \sigma_\mu^i \sigma_\nu^j \rangle. \quad (\text{D3})$$

Next, we perform a quantum-classical correspondence by associating a c -number with each of the spin operators, i.e. $\sigma_i^x \leftrightarrow s_i^x$, $\sigma_i^y \leftrightarrow s_i^y$ and $\sigma_i^z \leftrightarrow s_i^z$. The equations of motion for these c -numbers are obtained from the QLEs (D1) by replacing the quantum operators with their corresponding c -numbers. The quantum noise operators F_i^μ are replaced by c -number noise terms \mathcal{F}_i^μ .

We use symmetric correspondence to match the correlations of the c -number noise terms \mathcal{F}_i^μ with the correlations of the quantum noise operators F_i^μ , i.e.

$$\begin{aligned} \langle \mathcal{F}_i^\mu(t) \mathcal{F}_j^\nu(t') \rangle &= 2 \mathcal{D}_{ij}^{\mu\nu} \delta(t - t') \text{ with} \\ 2 \mathcal{D}_{ij}^{\mu\nu} &= D_{ij}^{\mu\nu} + D_{ji}^{\nu\mu}. \end{aligned} \quad (\text{D4})$$

The elements of the correlation matrix $2\mathcal{D}_{ij}^{\mu\nu}$ are summarized in Eq. (D5).

$$\begin{aligned}
2\mathcal{D}_{ii}^{xx} &= 2\mathcal{D}_{ii}^{yy} = 2(\Gamma_{ii}^- + \Gamma_{ii}^+) + \Gamma_{31} + (\Gamma_{13} + w) + \Gamma_d, \\
2\mathcal{D}_{ii}^{xy} &= 0, \\
2\mathcal{D}_{ii}^{zz} &= 2(w + \Gamma_{13} + \Gamma_{31} + 2(\Gamma_{ii}^- + \Gamma_{ii}^+)) \\
&\quad + 2(\Gamma_{31} + 2(\Gamma_{ii}^- - \Gamma_{ii}^+) - (w + \Gamma_{13})) \langle \sigma_i^z \rangle, \\
2\mathcal{D}_{ii}^{xz} &= (\Gamma_{31} + 2(\Gamma_{ii}^- - \Gamma_{ii}^+) - (w + \Gamma_{13})) \langle \sigma_i^x \rangle, \\
2\mathcal{D}_{ii}^{yz} &= (\Gamma_{31} + 2(\Gamma_{ii}^- - \Gamma_{ii}^+) - (w + \Gamma_{13})) \langle \sigma_i^y \rangle, \\
2\mathcal{D}_{ij}^{xx} &= 2\mathcal{D}_{ij}^{yy} = 2(\Gamma_{ij}^- + \Gamma_{ij}^+) \langle \sigma_i^z \sigma_j^z \rangle, \\
2\mathcal{D}_{ij}^{xy} &= 0, \\
2\mathcal{D}_{ij}^{zz} &= 2(\Gamma_{ij}^- + \Gamma_{ij}^+) (\langle \sigma_i^x \sigma_j^x \rangle + \langle \sigma_i^y \sigma_j^y \rangle), \\
2\mathcal{D}_{ij}^{xz} &= -2(\Gamma_{ij}^- + \Gamma_{ij}^+) \langle \sigma_i^z \sigma_j^x \rangle, \\
2\mathcal{D}_{ij}^{yz} &= -2(\Gamma_{ij}^- + \Gamma_{ij}^+) \langle \sigma_i^z \sigma_j^y \rangle.
\end{aligned} \tag{D5}$$

By construction, the diffusion matrix is symmetric,

and this property can be used to obtain the other elements. We simulate the $3N_\sigma$ c -number Langevin equations subject to the noise correlation matrix $2\mathcal{D}$ with elements given by Eq. (D5). Using vector notation, these stochastic differential equations (SDEs) can be written as

$$\frac{d}{dt} \vec{s}(t) = \vec{f}\{\vec{s}(t)\} + B(t)d\vec{W}, \tag{D6}$$

where the $\{dW_j\}$ are independent gaussian random variables with zero mean and variance dt . The function \vec{f} accounts for the drift part of the SDEs, while the matrix $B(t)$ is given by

$$\begin{aligned}
B &= \sqrt{2\mathcal{D}} = V\sqrt{\Lambda}V^{-1}, \quad \text{where} \\
2\mathcal{D} &= V\Lambda V^{-1}
\end{aligned} \tag{D7}$$

is the transformation that diagonalizes $2\mathcal{D}$ to the diagonal matrix Λ . We use an explicit second order weak scheme [44] to numerically integrate these SDEs.

-
- [1] D. Meiser, J. Ye, D. R. Carlson, and M. J. Holland, Phys. Rev. Lett. **102**, 163601 (2009).
- [2] D. Meiser and M. J. Holland, Phys. Rev. A **81**, 033847 (2010).
- [3] J. G. Bohnet, Z. Chen, J. M. Weiner, D. Meiser, M. J. Holland, and J. K. Thompson, Nature **484**, 78 (2012).
- [4] M. A. Norcia and J. K. Thompson, Phys. Rev. X **6**, 011025 (2016).
- [5] R. H. Dicke, Phys. Rev. **93**, 99 (1954).
- [6] H. Haffner, C. Roos, and R. Blatt, Physics Reports **469**, 155 (2008).
- [7] R. Blatt and C. F. Roos, Nat Phys **8**, 277 (2012).
- [8] J. W. Britton, B. C. Sawyer, A. C. Keith, C. C. J. Wang, J. K. Freericks, H. Uys, M. J. Biercuk, and J. J. Bollinger, Nature **484**, 489 (2012).
- [9] The analogy between a vibrational mode and an optical mode has been previously exploited to create a phonon laser with a single trapped ion; see K. Vahala, M. Herrmann, S. Knunz, V. Batteiger, G. Saathoff, T. W. Hansch, and T. Udem, Nat Phys **5**, 682 (2009).
- [10] A. Sørensen and K. Mølmer, Phys. Rev. Lett. **82**, 1971 (1999).
- [11] D. Leibfried, R. Blatt, C. Monroe, and D. Wineland, Rev. Mod. Phys. **75**, 281 (2003).
- [12] D. J. Larson, J. C. Bergquist, J. J. Bollinger, W. M. Itano, and D. J. Wineland, Phys. Rev. Lett. **57**, 70 (1986).
- [13] D. Kielpinski, B. E. King, C. J. Myatt, C. A. Sackett, Q. A. Turchette, W. M. Itano, C. Monroe, D. J. Wineland, and W. H. Zurek, Phys. Rev. A **61**, 032310 (2000).
- [14] M. D. Barrett, B. DeMarco, T. Schaetz, V. Meyer, D. Leibfried, J. Britton, J. Chiaverini, W. M. Itano, B. Jelenković, J. D. Jost, C. Langer, T. Rosenband, and D. J. Wineland, Phys. Rev. A **68**, 042302 (2003).
- [15] M. J. Biercuk, H. Uys, A. P. Vandevender, N. Shiga, W. M. Itano, and J. J. Bollinger, Quantum Information & Computation **9**, 920 (2009).
- [16] C. Monroe and J. Kim, Science **339**, 1164 (2013).
- [17] M. Kumph, M. Brownnutt, and R. Blatt, New Journal of Physics **13**, 073043 (2011).
- [18] Y. Lin, J. P. Gaebler, F. Reiter, T. R. Tan, R. Bowler, A. S. Sorensen, D. Leibfried, and D. J. Wineland, Nature **504**, 415 (2013), letter.
- [19] M. Xu and M. J. Holland, Phys. Rev. Lett. **114**, 103601 (2015).
- [20] A. Bermudez, T. Schaetz, and M. B. Plenio, Phys. Rev. Lett. **110**, 110502 (2013).
- [21] D. Meiser and M. J. Holland, Phys. Rev. A **81**, 063827 (2010).
- [22] J. I. Cirac, R. Blatt, P. Zoller, and W. D. Phillips, Phys. Rev. A **46**, 2668 (1992).
- [23] D. J. Wineland, C. Monroe, W. M. Itano, D. Leibfried, B. E. King, and D. M. Meekhof, J. Res. Natl. Inst. Stand. Tech. **103**, 259 (1998), arXiv:quant-ph/9710025 [quant-ph].
- [24] The analysis follows the classical treatment of normal modes discussed for eg. in H. Goldstein, C. Poole, and J. Safko, *Classical Mechanics* (Addison Wesley, 2002).
- [25] H. Carmichael, *Statistical Methods in Quantum Optics 1: Master Equations and Fokker-Planck Equations*, Physics and Astronomy Online Library (Springer, 1999).
- [26] E. M. Kessler, Phys. Rev. A **86**, 012126 (2012).
- [27] A. Klimov, J. Romero, J. Delgado, and L. Sánchez-Soto, Optics Communications **230**, 393 (2004).
- [28] B. C. Sawyer, J. W. Britton, A. C. Keith, C.-C. J. Wang, J. K. Freericks, H. Uys, M. J. Biercuk, and J. J. Bollinger, Phys. Rev. Lett. **108**, 213003 (2012).
- [29] W. M. Itano and D. J. Wineland, Phys. Rev. A **24**, 1364 (1981).

- [30] See V. Batteiger, S. Knünz, M. Herrmann, G. Saathoff, H. A. Schüssler, B. Bernhardt, T. Wilken, R. Holzwarth, T. W. Hänsch, and T. Udem, *Phys. Rev. A* **80**, 022503 (2009) for precision spectroscopy measurements of Mg^+ in zero magnetic field.
- [31] M. J. Biercuk, H. Uys, J. W. Britton, A. P. VanDevender, and J. J. Bollinger, *Nat Nano* **5**, 646 (2010).
- [32] C. Hempel, B. Lanyon, P. Jurcevic, R. Gerritsma, R. Blatt, and C. Roos, *Nat Photon* **7**, 630 (2013), letter.
- [33] P. Meystre and M. Sargent, *Elements of Quantum Optics* (Springer Berlin Heidelberg, 1998).
- [34] N. F. Ramsey, *Phys. Rev.* **78**, 695 (1950).
- [35] M. Xu, D. A. Tieri, and M. J. Holland, *Phys. Rev. A* **87**, 062101 (2013).
- [36] See J. Eschner, G. Morigi, F. Schmidt-Kaler, and R. Blatt, *J. Opt. Soc. Am. B* **20**, 1003 (2003) for a review of cooling methods in ion traps.
- [37] C. Monroe, D. M. Meekhof, B. E. King, S. R. Jefferts, W. M. Itano, D. J. Wineland, and P. Gould, *Phys. Rev. Lett.* **75**, 4011 (1995).
- [38] Y. Lin, J. P. Gaebler, T. R. Tan, R. Bowler, J. D. Jost, D. Leibfried, and D. J. Wineland, *Phys. Rev. Lett.* **110**, 153002 (2013).
- [39] R. Lechner, C. Maier, C. Hempel, P. Jurcevic, B. P. Lanyon, T. Monz, M. Brownnutt, R. Blatt, and C. F. Roos, *Phys. Rev. A* **93**, 053401 (2016).
- [40] See M. Xu, D. A. Tieri, E. C. Fine, J. K. Thompson, and M. J. Holland, *Phys. Rev. Lett.* **113**, 154101 (2014) for an analogous study in the cavity case.
- [41] M. Xu, S. B. Jäger, S. Schütz, J. Cooper, G. Morigi, and M. J. Holland, *Phys. Rev. Lett.* **116**, 153002 (2016).
- [42] For a concise introduction to superoperators see H. Carmichael, *Statistical Methods in Quantum Optics 2: Non-Classical Fields*, Theoretical and Mathematical Physics (Springer Berlin Heidelberg, 2010).
- [43] C. Cohen-Tannoudji, J. Dupont-Roc, and G. Grynberg, *Atom-photon interactions: basic processes and applications*, Wiley-Interscience publication (J. Wiley, 1992).
- [44] P. Kloeden and E. Platen, *Numerical Solution of Stochastic Differential Equations*, Stochastic Modelling and Applied Probability (Springer Berlin Heidelberg, 2011).